arXiv:1702.06644v1 [astro-ph.GA] 22 Feb 2017

Optical Spectra of Candidate International Celestial Reference Frame (ICRF) Flat-Spectrum Radio Sources. III

O. Titov

Geoscience Australia, PO Box 378, Canberra, ACT 2601, Australia

oleg.titov@ga.gov.au

T. Pursimo

Nordic Optical Telescope, Nordic Optical Telescope Apartado 474E-38700 Santa Cruz de La Palma, Santa Cruz de Tenerife, Spain

Helen M. Johnston

Sydney Institute for Astronomy, School of Physics, University of Sydney, NSW 2006, Australia

Laura M. Stanford

Geoscience Australia, PO Box 378, Canberra, ACT 2601, Australia

Richard W. Hunstead

Sydney Institute for Astronomy, School of Physics, University of Sydney, NSW 2006, Australia

David L. Jauncey

CSIRO Astronomy and Space Science, ATNF & Mount Stromlo Observatory, Cotter Road, Weston, ACT 2611, Australia

and

Katrina A. Zenere

School of Physics, University of Sydney, NSW 2006, Australia

Received _____; accepted _____

ABSTRACT

In extending our spectroscopic program, which targets sources drawn from the International Celestial Reference Frame (ICRF) Catalog, we have obtained spectra for ∼160 compact flat-spectrum radio sources and determined redshifts for 112 quasars and radio galaxies. A further 14 sources with featureless spectra have been classified as BL Lac objects. Spectra were obtained at three telescopes: the 3.58 m ESO New Technology Telescope (NTT), and the two 8.2 m Gemini telescopes in Hawaii and Chile. While most of the sources are powerful quasars, a significant fraction of radio galaxies is also included from the list of non-defining ICRF radio sources.

Subject headings: reference systems – galaxies: active – quasars: emission lines – BL Lacertae objects: general – radio continuum: general

1. Introduction

The accurate alignment of astronomical catalogues produced at different wavelengths is critical for confident identification of celestial objects. Milliarcsecond positions of compact extragalactic radio sources have been used since 1998 to define the International Celestial Reference Frame (ICRF; Ma, Arias & Eubanks 1998). The current realization of the International Celestial Reference System (ICRS; Arias et al. 1995) is the catalogue known as ICRF2 (Second Realization of the International Celestial Reference Frame). It is based on the progressive refinement since 1984 of the positions of a set of reference radio sources measured with Very Long Baseline Interferometry (VLBI) techniques (Ma et al. 2009, Fey et al. 2015). Some technical details are provided in our previous papers (Titov et al. 2011, 2013). The ICRF2 catalogue is based on the assumption that the reference radio sources have no significant proper motion, so their astrometric positions are affected only by the relativistic jets. However, at microarcsec levels Bastian (1995), Gwinn et al. (1997), Sovers, Fanselow & Jacobs (1998), and Kovalevsky (2003) have drawn attention to the effect of aberration in proper motions, while a dipole systematic of magnitude ~ 6 μas/year, detected by Titov, Lambert & Gontier (2011), Xu, Wang & Zhao (2012) and Titov & Lambert (2013), may degrade positions in the same way that proper motions of stars degraded the old optical catalogs.

The astrometric mission *Gaia* (Perryman et al. 2001; Mignard 2012), was launched on 2013 December 19 by the European Space Agency, and the first results have recently been published (Lindegren et al. 2016). One of the mission goals has been to measure high precision positions and proper motions of $\sim$500,000 quasars. A new astrometric reference frame based on the optical counterparts of the ICRF radio sources is being built, assuming that quasar parallaxes are zero (Michalik & Lindegren 2016). These new data will also test for the presence and magnitude of the dipole proper motion reported by Titov, Lambert

& Gontier (2011), Xu, Wang & Zhao (2012) and Titov & Lambert (2013), as well as any higher-order systematics. The alignment of radio and optical reference frames demands a reliable optical identification of the radio sources and, if possible, a redshift to confirm the identification. However, only approximately half of the ICRF radio sources have a measured redshift (Titov & Malkin 2009).

The reference radio sources are either optically bright quasars or extended radio galaxies. Our ongoing observing strategy first identifies the optical counterpart for each source, using either the SuperCOSMOS Sky Survey (Hambly et al. 2001) or the Sloan Digital Sky Survey (DR9 through 13) (SDSS; York et al. 2000), and we then obtain a spectrum to secure a redshift. We routinely obtain a short-exposure wideband image of the field prior to starting the spectroscopic exposure, firstly to confirm the identification and secondly to guard against possible confusion by foreground stars, especially in crowded fields (e.g., see Titov et al. 2013, Fig. 3); good seeing is a critical issue in the latter case.

The current paper, Part III of our ongoing project, presents redshifts for 112 targets, mostly in the southern hemisphere. The majority appear point-like in the optical with broad permitted lines or BL Lac objects with featureless spectra; only two clear galaxies with narrow emission lines are presented, although classification of images near the limiting magnitudes of the optical surveys is difficult. We describe the observations and data reduction procedures in Section 2. Our spectra, along with detailed comments on individual sources, are presented in Section 3. A discussion of targets showing interesting emission or absorption properties is given in Section 4, followed by a summary and conclusion in Section 5. Where relevant, a ΛCDM cosmology has been assumed, with $H_0 = 70$ km s^{-1} Mpc^{-1}, $\Omega_M = 0.29$ and $\Omega_\Lambda = 0.71$.

2. Observations

Spectroscopic observations were carried out at three optical facilities.

ESO NTT. We had a 5-night observing run in Visitor Mode at the European Southern Observatory (ESO) 3.58 m New Technology Telescope (NTT) in 2013 December (Proposal 092.A-0021 (A)) using the ESO Faint Object Spectrograph and Camera (EFOSC) system with grism #13 covering the wavelength range 3685–9315 Å. The seeing during observations was typically $0\farcs5 - 2\farcs0$, with a spectral resolution 21 Å FWHM. Exposure times varied from 5–30 minutes depending on the magnitude of each target and current sky conditions. Wavelength calibration made use of HeNeAr comparison spectra, resulting in an rms accuracy of 0.5 Å.

Gemini: A large number of targets were observed in Service Mode at the Gemini North and Gemini South 8.2 m telescopes through the Poor Weather Program (Proposals GN-2012B-Q-127, GS-2013A-Q-99, GS-2014A-Q-93) using the Gemini Multi-Object Spectrograph (GMOS) system with grating R400 at each site. This grating covers 4500 Å centered at 5200 Å. The wavelength resolution was ∼15 Å FWHM, and an exposure time of 20 minutes was used for all targets. Wavelength calibration used the spectra of a CuAr comparison lamp, giving an rms accuracy of 0.3 Å.

Data reduction was performed with the IRAF software suite[1] using standard procedures for spectral analysis. Bias and flat-field correction was applied to each frame, and cosmic rays were removed using the IRAF task SZAP. Where more than one exposure was obtained, the separate exposures were combined. After spectrum extraction, sky subtraction and

[1]IRAF is distributed by the National Optical Astronomical Observatory, which is operated by the Association of Universities for Research in Astronomy, Inc., under contract to the National Science Foundation.

wavelength calibration, the final one-dimensional spectra were flux-calibrated with a spectrophotometric standard observed with the same instrumental setup. Because the observing conditions were often non-photometric, especially for Gemini observations made through the Poor Weather Program, the flux calibration should be taken as approximate.

3. Results

We present our spectroscopic results in the same format as our previous paper (Titov et al. 2013). The redshifts of 112 IVS objects are listed in Table 1, along with their J2000 ICRF2 positions (Ma et al. 2009, Fey et al. 2015), the telescope used for each spectrum, the identified emission lines (rest and observed wavelengths), the mean redshift and error, and brief notes on individual sources. Additional notes on individual sources, marked with an asterisk in the final column, are given in Section 3.1. The quoted errors in the mean redshift $\overline{z}$ were calculated as discussed in Titov et al. (2013), i.e., from the quadratic combination of the scatter in the redshift estimates and the fractional error in the wavelength calibration. Single-line redshifts, usually Mg II, are assigned an uncertainty of $\Delta z = 0.001$ if the signal-to-noise (S/N) is high, increasing to 0.003 for low S/N, or a broad or asymmetric line.

Figure 1 displays the individual spectra, along with the line identifications. Blue dashed lines indicate lines that were used for redshift calculation, while red dot-dashed line indicates lines that were present, generally at a low S/N, but not used in determining the mean redshift. Telluric lines near 6850 Å and 7600 Å are marked on the spectra.

Fourteen objects with good S/N ratio and featureless spectra were classed as probable BL Lac objects. They are listed in Table 2 with their ICRF2 positions (Ma et al. 2009, Fey et al. 2015), and their spectra are shown in Figure 2. Comments on two of them are included in Section 3.1. There is also a significant fraction of quasars in Fig. 1 with weak

emission lines on a strong continuum (e.g. IVS B0530−484 and B0619−468), which we assume are incipient BL Lacs, perhaps not surprising in a VLBI-selected sample.

An additional 23 targets had low S/N spectra that did not permit a confident spectral classification. These are listed in Table 3 with their ICRF2 positions. Attempts to identify and obtain redshifts for 11 IVS targets at low Galactic latitude were not successful.

3.1. Notes on individual targets

1. IVS B0023−354—intervening absorption system at $z_{\rm abs} = 1.3167 \pm 0.0010$ with lines of Fe II $\lambda\lambda$2586, 2600, Mg II $\lambda\lambda$2796, 2803 and Mg I λ2852. Although the Mg II doublet is not resolved, the presence of Mg I and Fe II confirm the system.

2. IVS B0048+447—two associated absorption systems are detected within the Mg II emission line, one at $z_{\rm abs} = 1.2568 \pm 0.0001$ and the other, including Mg I λ2852, at $z_{\rm abs} = 1.2715 \pm 0.0001$. Their velocities relative to the Mg II emission line are -370 and $+2300\,{\rm km\,s^{-1}}$, respectively.

3. IVS B0229+262—a possible intervening C IV $\lambda\lambda$1548, 1550 doublet is detected at $z_{\rm abs} = 2.5261 \pm 0.0001$.

4. IVS B0307−085—very strong associated absorption in C IV $\lambda\lambda$1548, 1550, Si IV $\lambda\lambda$1393, 1402, N V $\lambda\lambda$1238, 1242 and Lyα λ1215 at a redshift of $z_{\rm abs} = 3.2899 \pm 0.0005$, consistent with zero velocity shift relative to emission.

5. IVS B0521−403—probable intervening absorption system at $z_{\rm abs} = 0.6974 \pm 0.0001$ based on Mg II $\lambda\lambda$2796, 2803 (blend) and Mg I λ2852 lines. Spectral resolution is too low to separate the Mg II doublet, but the wavelength match is good. There are two further absorption lines at 5023Å and 5997Å, which could not be identified but may

be additional blended Mg II doublets based on their line widths.

6. IVS B0550−453—intervening absorption system at $z_{\rm abs} = 0.6859 \pm 0.0001$ based on lines of Fe II $\lambda\lambda$2344, 2382, 2586+2600 (blend) and Mg II $\lambda\lambda$2796, 2803 (blend).

7. IVS B0722−068—broad emission from Fe II multiplets both blueward and redward of Hβ (see Fig. 5).

8. IVS B0727−365—permitted lines Mg II, Hγ and Hβ are displaced $\sim$1200 km s^{-1} to higher redshift relative to the forbidden lines; the overall mean redshift is given in Table 1.

9. IVS B0838−573—absorption line at 6237 Å is a possible intervening Mg II doublet at $z_{\rm abs} = 1.2304$.

10. IVS B0858−313—broad emission from Fe II multiplets both blueward and redward of Hβ; [O III] λ5007 may be partly blended with Fe II λ5018 (see Fig. 5).

11. IVS B0917−354—broad emission from Fe II multiplets both blueward and redward of Hβ; [O III] λ5007 may be partly blended with Fe II λ5018 (see Fig. 5).

12. IVS B1006−093—probable blend of associated Mg II $\lambda\lambda$2796, 2803 absorption at $z_{\rm abs} = 1.1884 \pm 0.0001$.

13. IVS B1219−457—prominent broad absorption line in the blue wing of Mg II emission at $z_{\rm abs} = 1.034$, corresponding to an outflow velocity of $\sim$2600 km s^{-1}.

14. IVS B1228−352—absorption line at 4151 Å is a possible intervening Mg II doublet at $z_{\rm abs} = 0.4845$.

15. IVS B1229−123—self-absorption in C IV $\lambda\lambda$1548, 1550 is matched by absorption in Lyα λ1215 at $z_{\rm abs} = 2.1054 \pm 0.0003$.

16. IVS B1418−481—intervening absorption system at $z_{\rm abs} = 1.0393 \pm 0.0001$ is based on Mg II $\lambda\lambda$2796, 2803 and Mg I λ2853.

17. IVS B1558−072—bright quasar with an intervening absorption system at $z_{\rm abs} = 1.0787 \pm 0.0001$ based on lines of Fe II $\lambda\lambda$2344, 2382, 2586, 2600 and Mg II $\lambda\lambda$2796, 2803.

18. IVS B1711−670 (Fig. 2)—observed in poor seeing and we assume that the close star 2.″5 to the south-west is responsible for contamination by weak Hα and Hβ absorption at rest. Spectrum otherwise is featureless and the target is tentatively classified as a BL Lac object.

19. IVS B1712+530—bright quasar with an intervening absorption system at $z_{\rm abs} = 1.5145 \pm 0.0010$ based on lines of Fe II $\lambda\lambda$2586, 2600 and Mg II $\lambda\lambda$2796, 2803.

20. IVS B1810−745—self-absorption near the centre of C IV emission at $z_{\rm abs} = 2.246$.

21. IVS B1813−497—spectrum was obtained in poor seeing and is partly contaminated by light from a close star ∼0.8 arcsec west of the quasar; see Fig. 3.

22. IVS B1905−252—intervening absorption system at $z_{\rm abs} = 1.3165 \pm 0.0001$ based on Fe II λ2600 and Mg II $\lambda\lambda$2796, 2803.

23. IVS B1957−423—absorption system, probably associated, at $z = 0.9674 \pm 0.0001$ in the extreme blue wing of Mg II emission, based on Mg II $\lambda\lambda$2796, 2803 and Fe II λ2600; the blueshift is ∼3200 km s^{-1}.

24. IVS B2029−215—an FeLoBAL quasar, with very strong broad absorption and emission, predominantly in Fe II; see Section 4.3 and Fig. 6.

25. IVS B2036−034—intervening absorption system at $z_{\rm abs} = 1.2097 \pm 0.0010$ based on lines of Fe II $\lambda\lambda$2344, 2382, 2586, 2600 and Mg II $\lambda\lambda$2796, 2803.

26. IVS B2044−188—intervening absorption system at $z_{\rm abs} = 1.4905 \pm 0.0010$ based on lines of Fe II $\lambda\lambda$2344, 2382, 2586, 2600, Mg II $\lambda\lambda$2796, 2803 and Mg I λ2852.

27. IVS B2107−553—the two absorption lines, at 4747.2Å and 4801.1Å can not be identified with any known doublet or pair of lines.

28. IVS B2131−690—very broad emission lines of C III] and Mg II.

29. IVS B2132−638—prominent associated Mg II $\lambda\lambda$2796, 2803 absorption close to the peak of the emission line at $z = 1.5349 \pm 0.0001$ with a blueshift of $\sim$250 km s^{-1}.

30. IVS B2155−475—two absorption line systems: an intervening Mg II $\lambda\lambda$2796, 2803 system at $z = 0.7292 \pm 0.0044$, and an associated system at $z = 1.7423 \pm 0.0010$ based on Si II λ1526, C IV $\lambda\lambda$1548, 1550 (blend), C I λ1560 and Fe II λ1608.

31. IVS B2257+313 (Fig. 2)—featureless spectrum with a clear absorption system at $z_{\rm abs} = 0.9317 \pm 0.0001$ defined by lines of Fe II $\lambda\lambda$2586, 2600 and Mg II $\lambda\lambda$2796, 2803, thereby setting a lower limit on the redshift of this BL Lac object.

32. IVS B2300+386—two intervening absorption systems at $z_{\rm abs} = 1.0138 \pm 0.0001$ and $z_{\rm abs} = 1.6005 \pm 0.0001$ based solely on the Mg II $\lambda\lambda$2796, 2803 doublet.

33. IVS B2313−182—low-luminosity radio galaxy with narrow [O II] λ3727 and [O III] $\lambda\lambda$4959, 5007 emission on a predominantly stellar continuum with clear Ca II absorption.

3.2. Separation of close objects

Galactic stars are occasionally found close on the sky to the VLBI radio position, either contaminating the spectrum or so closely aligned with the radio source that the

field is completely obscured. Of the three examples shown in Fig. 3, redshifts were able to be recovered for IVS B0905−202 and B1813−497, although the latter spectrum, taken in poor seeing, is clearly contaminated by stellar absorption lines at rest. In the case of IVS B0758−737, which is relatively bright on VLBI baselines, there is also the opportunity to monitor changes with time in the VLBI position as proper motion of the foreground star changes the gravitational deflection of the quasar light.

4. Discussion

The longer integration times in the present dataset have brought to light some spectral features, both in emission and absorption, that were either not detectable in the earlier datasets or extremely rare (Titov et al. 2011, 2013). These are discussed briefly in the following sections.

4.1. Mg II absorption systems

The generally good S/N has allowed the detection of a number of absorption systems, both those associated with the target quasar and those intervening along the line of sight. The resolution of the NTT spectra is not sufficient to separate the Mg II doublet, but in most cases the system is confirmed by the presence of other lines, notably Mg I and/or Fe II. Absorption line redshifts were determined using SPLOT or SPECFIT in IRAF. Gaussian profiles were fitted to the lines, assuming a single redshift and width for all lines. Redshifts span the range $z_{\rm abs} = 0.7$–1.5.

A montage of the Mg II systems shifted to the rest frame is shown in Fig. 4. The NTT spectral resolution is too low to separate the Mg II doublet and Fig. 4 only includes those NTT systems with confirming lines of Mg I and/or Fe II. Mg II doublet ratios in the

Gemini spectra are all close to 1, indicating that the doublet is at, or close to, saturation with equivalent widths $W_0^{\lambda 2796} > 0.5$Å.

The principal interest in IVS quasars showing strong Mg II absorption, both associated and intervening, is their value as potential targets in searches for redshifted neutral hydrogen, taking advantage of the similar excitation potentials (and therefore locations) of H I and Mg II. While our sample is small in comparison with those from the Sloan Digital Sky Survey (eg. Nestor et al. 2005), the majority of the Sloan sample is radio quiet. Moreover, ICRF source selection ensures that a substantial fraction of the radio flux density is contained within a few milliarcsec, thereby increasing the likelihood of an H I detection. Source selection played an important role in the first successful detection of redshifted H I with the Australian SKA Pathfinder (ASKAP; Johnston et al. 2007) where the target was the peaked spectrum VLBI source IVS B1740−517 (Allison et al. 2015) at $z = 0.44$; unfortunately, the optical spectrum, obtained at Gemini South through Director's Discretionary Time, did not cover the Mg II line.

4.2. Fe II emission near Hβ

Three of the low-z quasars show prominent Fe II multiplet emission near Hβ: IVS B0722−068, B0858−313 and B0917−354. A montage of these three spectra, reduced to the emission rest frame, is shown in Fig. 5. Fe II emission in this spectral region was first noted and analysed by Wampler & Oke (1967) in the spectrum of 3C 273. They noted how the λ4924 line could distort the red wing of the Hβ profile and the λ5018 line could blend with [O III] λ5007.

4.3. The FeLoBAL quasar IVS B2029−215

An extreme example of broad Fe II emission and absorption is shown in the spectrum of the quasar, IVS B2029−215, which is dominated by broad Fe II emission and absorption lines. This object belongs to a rare class of low-ionization broad absorption line quasars known as FeLoBALs, so-named because the spectrum is dominated by excited states of Fe II. The spectrum, shifted to the emission rest frame, is shown in Fig. 6.

The spectrum of IVS B2029−215 is very similar to that of the $z = 0.692$ quasar FIRST J121442.3+280329 (de Kool et al. 2002; Branch et al. 2002) from the FIRST Bright Quasar Survey (White et al. 2000). By analogy with the spectrum of FIRST J121442.3+280329 (de Kool et al. 2002) we show a tentative continuum in Fig. 6 on the assumption that broad emission and blue-shifted broad absorption are superimposed on a power-law continuum from the accretion disk. The IVS B2029−215 continuum, however, is substantially redder than that of FIRST J121442.3+280329, suggesting the presence of dust in the outflowing gas.

4.4. Continuum absorption below Lyα

It is well known that the continuum level in high redshift quasars is depressed below Lyα relative to an extrapolation of the level above Lyα. The fractional depression, D_A, of the continuum between Lyα and Lyβ increases with redshift due mainly to the increasing density of absorption lines of the Lyα forest, with additional contributions from heavy-element lines and, at the highest redshifts, distributed neutral hydrogen (e.g. Jenkins & Ostriker 1991.)

In the present sample there are 8 quasars with $z > 2.6$ and good spectral coverage down to Lyβ. Of these, five show the expected continuum depression below Lyα but three,

IVS B0407−129, B1020−045 and B1044−512, have $D_A \approx 0$. The latter three spectra, all at $z \sim 2.6$, were obtained at the NTT in visitor mode and the spectral response has been well calibrated with standard star observations. The implication is that these sightlines have a lower density of Lyα forest lines, and/or a more highly ionized intergalactic medium. To follow up these possibilities, we are planning to observe the region well below Lyα in these quasars at higher spectral resolution and signal-to-noise.

5. Summary and conclusion

We present redshifts and spectra of a further 112 emission-line objects identified with VLBI radio sources drawn from the candidate International Celestial Reference Catalog. As in our previous papers (Titov et al. 2011, 2013) the chosen targets were mostly in the south so as to improve the uniformity across the two hemispheres. Redshifts were generally based on two or more emission lines, but single-line redshifts, all Mg II, were considered reliable on the basis of other spectral information. There were 14 objects with high S/N but featureless spectra that we classified as probable BL Lac objects, while a further 22 had S/N too low for reliable classification.

The majority of spectra show the broad permitted lines and power-law continua characteristic of quasars, but the sample does include two low-redshift galaxies with only narrow forbidden lines and stellar continua. Morphological differentiation is difficult at redshifts $z > 0.5$.

Amongst the sample of 112 spectra, we identify 17 low-redshift Mg II absorbers, both associated and intervening. Because these absorbers are seen against very compact radio sources, they are potential targets for H I absorption searches with next generation radio telescopes.

This paper is based on data collected at three telescopes:

1. ESO NTT, under the European Organisation for Astronomical Research in the Southern Hemisphere, Chile under program 092.A-0021 (A)

2. Two Gemini Observatories, which are operated by the Association of Universities for Research in Astronomy, Inc., under a cooperative agreement with the National Science Foundation on behalf of the Gemini partnership: the National Science Foundation (United States), the Science and Technology Facilities Council (United Kingdom), the National Research Council (Canada), CONICYT (Chile), the Australian Research Council (Australia), Ministério da Ciência, Tecnologia, Inovações e Comunicações (Brazil) and Ministerio de Ciencia, Tecnología e Innovación Productiva (Argentina) under programs GS-2013A-Q-99 and GS-2014A-Q-93 (Gemini South), and GN-2012B-Q-127 (Gemini North).

Funding for SDSS-III has been provided by the Alfred P. Sloan Foundation, the Participating Institutions, the National Science Foundation and the U.S. Department of Energy Office of Science. The SDSS-III web site is http://www.sdss3.org/.

SDSS-III is managed by the Astrophysical Research Consortium for the Participating Institutions of the SDSS-III Collaboration including the University of Arizona, the Brazilian Participation Group, Brookhaven National Laboratory, University of Cambridge, Carnegie Mellon University, University of Florida, the French Participation Group, the German Participation Group, Harvard University, the Instituto de Astrofisica de Canarias, the Michigan State/Notre Dame/JINA Participation Group, Johns Hopkins University, Lawrence Berkeley National Laboratory, Max Planck Institute for Astrophysics, Max Planck Institute for Extraterrestrial Physics, New Mexico State University, New York University, Ohio State University, Pennsylvania State University, University of Portsmouth,

Princeton University, the Spanish Participation Group, University of Tokyo, University of Utah, Vanderbilt University, University of Virginia, University of Washington, and Yale University.

The paper is published with the permission of the CEO, Geoscience Australia

REFERENCES

Allison, J. R., Sadler, E. M., Moss, V. A., et al. 2015, MNRAS, 453, 1249

Arias, E. F., Charlot, P., Feissel, M., & Lestrade, J.-F. 1995, A&A, 303, 604

Bastian, U. 1995, in M. Perryman & F. van Leeuwen (ed.), RGO-ESA Workshop ESA SP-379, 99

Branch, D., Leighly, K. M., Thomas, R. C., & Baron, E., 2002, ApJ, 578, L37

de Kool, M., Becker, R. H., Gregg, M. D., et al. 2002, ApJ, 567, 58

Fey, A., et al. 2015, AJ, 150, 58

Gwinn, C. R., Eubanks, T. M., Pyne, T. et al., 1997, ApJ, 485, 87

Hambly, N. C., Davenhall, A. C., Irwin, M. J., & MacGillivray, H. T., 2001, MNRAS, 326, 1315

Jenkins, E. B. & Ostriker, J. P. 1991, ApJ, 376, 33

Johnston, S. et al. 2007, PASA, 24, 174

Kovalevsky, J. 2003, A&A, 404, 743

Lindegren, L., et al. 2016, A&A, 595, A4

Ma, C., Arias, E. F., & Eubanks, T. M., 1998, AJ, 116, 516

Ma, C. et al. 2009, in Fey, A., Gordon, G., & Jacobs, C. (ed.), IERS Technical Note No. 35, Frankfurt am Main: Verlag des Bundesamts für Kartographie und Geodäsie

Michalik, D. & Lindegren, L. 2016, A&A, 586, A26

Mignard, F., 2012, Proc. 11th European VLBI Network Symposium, October, 2012.

Nestor, D. B., Turnshek, D. A., & Rao, S. M., ApJ, 628, 637

Perryman, M. A. C., de Boer, K. S., Gilmore, G., et al. 2001, A&A, 369, 339

Sovers, O. J., Fanselow, J. L. & Jacobs, C. S., 1998, Rev Mod Phys., 70, 1393

Titov, O., & Malkin, Z. 2009, A&A, 506, 1477

Titov, O., Jauncey, D. L, Johnston, H. M., et al. 2011, AJ, 142, 165

Titov, O., Lambert, S. B., & Gontier, A.-M., 2011, A&A, 529, 91

Titov, O., Stanford. L. M., Johnston, H. M., et al. 2013, AJ, 146, 10

Titov, O., & Lambert, S., 2013, A&A, 559, 95

Wampler, E. J. & Oke, J. B. 1967, ApJ, 148, 695

White, R. L., et al. 2000, ApJS. 126, 133

Xu, M. H., Wang, G. L., & Zhao, M., 2013, A&A, 534, 212

York, D. G., Adelman, J., Anderson, J. E., Jnr, et al. 2000, AJ, 120, 1579

This manuscript was prepared with the AAS LaTeX macros v5.2.

Table 1. Observed emission lines

Source	RA (J2000)[a]	Dec (J2000)[a]	Telescope[b]	Line	Rest λ	Obs λ[c]	z	Note[d]
IVS B0001−440	00 04 07.2575	−43 45 10.146	GS	Mg II	2799.9	5582.9	0.994 ± 0.001	S *
IVS B0009+081	00 11 35.2696	+08 23 55.586	GN	C III]	1908.7	4587.4	1.4032 ± 0.0003	
				Mg II	2799.9	6728.1		
IVS B0010−873	00 11 51.4792	−87 06 25.453	GS	Lyα	1215.7	5218.9	3.2928 ± 0.0026	
				N V	1240.1	5329.9		
				Si II	1304.4	5601.8		
				C II	1334.5	[5737.4]		
				Si IV	1398.3	[5985.2]		
				C IV	1549.5	6640.6		
IVS B0016−223	00 19 22.8280	−22 05 27.938	GS	Mg II	2799.9	4637.1	0.6559 ± 0.0003	
				[Ne V]	3345.4	5536.8		
				[Ne V]	3425.5	5674.5		
				[O II]	3726.8	6172.2		
				[Ne III]	3868.7	6405.2		
				[Ne III]	3967.4	[6571.1]		
				Hδ	4101.7	[6789.1]		

Table 1—Continued

Source	RA (J2000)[a]	Dec (J2000)[a]	Telescope[b]	Line	Rest λ	Obs λ[c]	z	Note[d]
				Hγ	4340.5	[7182.6]		
				[O III]	4363.2	[7219.4]		
IVS B0023−354	00 26 16.3871	−35 12 48.789	NTT	C IV	1549.5	4625.7	1.996 ± 0.005	*
				C III]	1908.7	5730.0		
				Mg II	2799.9	8397.9		
IVS B0048+447	00 51 36.4736	+44 59 35.958	GN	Mg II	2799.9	6311.7	1.254 ± 0.001	S *
IVS B0105+129	01 07 45.9618	+13 12 05.191	GN	Mg II	2799.9	4929.9	0.7600 ± 0.0002	
				[Ne V]	3345.4	5885.5		
				[Ne V]	3425.5	6028.7		
				[O II]	3726.8	6558.7		
				[Ne III]	3868.7	6808.6		
				[Ne III]	3967.4	6982.7		
				Hδ	4101.7	[7217.5]		
IVS B0117−171	01 19 43.6459	−16 54 08.972	GS	Mg II	2799.9	4881.3	0.7440 ± 0.0005	
				[Ne V]	3425.5	[5980.1]		
				[O II]	3726.8	6503.4		

Table 1—Continued

Source	RA (J2000)[a]	Dec (J2000)[a]	Telescope[b]	Line	Rest λ	Obs λ[c]	z	Note[d]
				[Ne III]	3868.7	6745.1		
IVS B0134+215	01 37 15.6249	+21 45 44.270	GN	Mg II	2799.9	5842.7	1.0864 ± 0.0004	
				[Ne V]	3425.5	7145.6		
IVS B0137-273	01 39 55.3988	−27 05 29.107	NTT	Lyα	1215.7	[5097.2]	3.147 ± 0.005	
				Si IV	1398.3	5811.4		
				C IV	1549.5	6412.1		
				C III]	1908.7	7912.0		
IVS B0158+096	02 01 15.4974	+09 54 54.392	GN	Mg II	2799.9	6324.8	1.259 ± 0.001	S
IVS B0159−668	02 01 07.7442	−66 38 12.665	NTT	C III]	1908.7	4339.2	1.279 ± 0.006	
				Mg II	2799.9	6394.2		
IVS B0200+30A	02 03 44.2706	+30 42 37.836	GN	Mg II	2799.9	4928.3	0.7598 ± 0.0002	
				[Ne V]	3425.5	6026.3		
				[O II]	3726.8	6559.3		
				[Ne III]	3868.7	6806.6		
				[Ne III]	3967.4	6982.2		
IVS B0224−189	02 26 47.6283	−18 43 39.238	GS	C IV	1549.5	4129.6	1.679 ± 0.013	

Table 1—Continued

Source	RA (J2000)[a]	Dec (J2000)[a]	Telescope[b]	Line	Rest λ	Obs λ[c]	z	Note[d]
				C III]	1908.7	5138.1		
IVS B0228−624	02 30 11.5749	−62 14 35.714	NTT	Si IV	1398.3	[3799.1]	1.6932 ± 0.0026	
				C IV	1549.5	4176.5		
				C III]	1908.7	5130.6		
				Mg II	2799.9	7548.7		
IVS B0229+262	02 32 27.6232	+26 28 38.590	GN	Lyα	1215.7	4584.3	2.7720 ± 0.0005	
				N V	1240.1	[4683.2]		
				Si IV	1398.3	[5273.4]		
				C IV	1549.5	5845.7		
				He II	1640.4	6187.1		
				C III]	1908.7	7201.1		
IVS B0230−288	02 32 36.7412	−28 39 26.306	NTT	Mg II	2799.9	5607.4	1.003 ± 0.002	S
				H δ	4101.7	[8230.9]		
IVS B0234+469	02 38 16.5032	+47 12 18.551	GN	Mg II	2799.9	4956.2	0.7695 ± 0.0007	
				[O II]	3726.8	6592.0		
				Hδ	4101.7	[7262.3]		

Table 1—Continued

Source	RA (J2000)[a]	Dec (J2000)[a]	Telescope[b]	Line	Rest λ	Obs λ[c]	z	Note[d]
IVS B0244+327	02 47 41.2322	+32 54 31.836	GN	C III]	1908.7	5185.0	1.7165 ± 0.0003	
				Mg II	2799.9	[7589.0]		
IVS B0307−085	03 10 02.0490	−08 23 39.297	GS	Lyα	1215.7	5224.5	3.289 ± 0.005	*
				N V	1240.1	[5324.5]		
				Si IV	1398.3	5998.1		
				C IV	1549.5	6630.5		
IVS B0307−362	03 09 02.5107	−36 04 03.746	GS	C III]	1908.7	4206.1	1.2051 ± 0.0015	
				Mg II	2799.9	6178.3		
IVS B0322−555	03 24 05.5484	−55 20 54.140	GS	Lyα	1215.7	3861.9	2.1780 ± 0.0007	
				Si IV	1398.3	4442.6		
				C IV	1549.5	4923.4		
				He II	1640.4	5212.5		
				Si III]	1890.0	6012.5		
				C III]	1908.7	6065.6		
IVS B0324−379	03 26 03.0004	−37 46 09.181	NTT	Mg II	2799.9	5247.1	0.8749 ± 0.0014	
				[Ne V]	3425.5	6418.9		

Table 1—Continued

Source	RA (J2000)[a]	Dec (J2000)[a]	Telescope[b]	Line	Rest λ	Obs λ[c]	z	Note[d]
				[O II]	3726.8	6979.3		
				Hγ	4340.5	8156.0		
IVS B0325−182	03 27 43.3416	−18 03 42.027	NTT	Mg II	2799.9	4841.2	0.7303 ± 0.0004	
				Hδ	4101.7	7099.0		
				Hγ	4340.5	7513.9		
				Hβ	4861.3	8413.7		
				[O III]	5006.8	8659.6		
IVS B0407−129	04 10 13.9529	−12 51 11.209	NTT	Lyβ	1025.7	[3768.0]	2.649 ± 0.004	
				Lyα	1215.7	[4470.3]		
				Si IV	1398.3	5108.1		
				C IV	1549.5	5642.9		
				C III]	1908.7	6969.9		
IVS B0423+297	04 26 30.2261	+29 52 22.933	GN	C IV	1549.5	5087.9	2.291 ± 0.007	
				C III]	1908.7	6295.6		
IVS B0431−642	04 31 28.1028	−64 06 31.366	NTT	Si IV	1398.3	4094.3	1.9263 ± 0.0023	
				C IV	1549.5	4527.8		

Table 1—Continued

Source	RA (J2000)[a]	Dec (J2000)[a]	Telescope[b]	Line	Rest λ	Obs λ[c]	z	Note[d]
				C III]	1908.7	5579.3		
				Mg II	2799.9	8209.5		
IVS B0511−203	05 13 42.8583	−20 16 11.487	NTT	C IV	1549.5	3861.4	1.487 ± 0.004	
				C III]	1908.7	4732.5		
				Mg II	2799.9	6974.2		
IVS B0521−403	05 22 54.1151	−40 20 30.941	NTT	C III]	1908.7	4549.7	1.380 ± 0.004	*
				Mg II	2799.9	6652.6		
IVS B0530−484	05 31 58.6151	−48 27 35.972	NTT	Mg II	2799.9	5073.2	0.8116 ± 0.0003	
				[O II]	3726.8	6750.4		
IVS B0538−562	05 39 42.3928	−56 12 49.967	NTT	C III]	1908.7	4236.8	1.224 ± 0.004	
				Mg II	2799.9	6239.5		
IVS B0550−453	05 52 10.0402	−45 22 24.671	NTT	Mg II	2799.9	5039.0	0.8011 ± 0.0004	*
				[Ne V]	3425.5	6165.5		
				[O II]	3726.8	6710.6		
				[Ne III]	3868.7	6971.9		
				Hϵ	3970.1	7144.7		

Table 1—Continued

Source	RA (J2000)[a]	Dec (J2000)[a]	Telescope[b]	Line	Rest λ	Obs λ[c]	z	Note[d]
				Hδ	4101.7	7394.8		
				Hγ	4340.5	7825.8		
				Hβ	4861.3	8757.9		
				[O III]	4958.9	8930.9		
				[O III]	5006.8	[9015.2]		
IVS B0606−025	06 09 28.5116	−02 30 52.931	NTT	Mg II	2799.9	4588.7	0.6362 ± 0.0010	
				[O II]	3726.8	6091.0		
				[O III]	4958.9	8111.8		
				[O III]	5006.8	8188.9		
IVS B0619−468	06 21 19.4363	−46 49 58.438	NTT	C III]	1908.7	4214.9	1.2105 ± 0.0023	
				Mg II	2799.9	6195.5		
IVS B0704−231	07 06 33.5180	−23 11 37.846	NTT	Mg II	2799.9	4742.3	0.6918 ± 0.0006	
				[Ne V]	3345.4	5655.5		
				[Ne V]	3425.5	5790.7		
				[O II]	3726.8	6300.7		
				[Ne III]	3868.7	6544.0		

Table 1—Continued

Source	RA (J2000)[a]	Dec (J2000)[a]	Telescope[b]	Line	Rest λ	Obs λ[c]	z	Note[d]
				[Ne III]	3967.4	6707.2		
				Hγ	4340.5	7361.9		
				[O III]	4363.2	7378.9		
				Hβ	4861.3	8233.0		
				[O III]	4958.9	8384.9		
				[O III]	5006.8	8466.4		
IVS B0705−412	07 06 43.0598	−41 22 23.785	NTT	C IV	1549.5	4007.5	1.5868 ± 0.0021	
				He II	1640.4	4239.8		
				C III]	1908.7	4930.9		
				Mg II	2799.9	7259.6		
IVS B0722−068	07 24 29.1437	−06 58 07.734	NTT	Mg II	2799.9	4161.5	0.4871 ± 0.0004	
				Hγ	4340.5	6458.1		
				Hβ	4861.3	7231.7		
				[O III]	5006.8	7444.2		
IVS B0727−365	07 29 05.4122	−36 39 45.244	NTT	Mg II	2799.9	4497.6	0.6027 ± 0.0011	*
				[Ne V]	3425.5	5487.2		

Table 1—Continued

Source	RA (J2000)[a]	Dec (J2000)[a]	Telescope[b]	Line	Rest λ	Obs λ[c]	z	Note[d]
				[O II]	3726.8	5962.0		
				[Ne III]	3868.7	6190.9		
				[Ne III]	3967.4	6349.5		
				Hγ	4340.5	6977.1		
				Hβ	4861.3	7811.6		
				[O III]	4958.9	7937.4		
				[O III]	5006.8	8013.7		
IVS B0734−044	07 36 33.6271	−04 33 11.859	NTT	C IV	1549.5	3888.9	1.5117 ± 0.0027	
				C III]	1908.7	4787.5		
				Mg II	2799.9	7047.3		
IVS B0748−069	07 50 47.1484	−07 06 04.025	NTT	Si IV	1398.3	3865.6	1.7624 ± 0.0023	
				C IV	1549.5	4284.0		
				C III]	1908.7	5263.8		
				Mg II	2799.9	[7764.0]		
IVS B0804−267	08 06 12.7225	−26 52 33.308	NTT	C III]	1908.7	4257.6	1.2302 ± 0.0004	
				Mg II	2799.9	6243.3		

Table 1—Continued

Source	RA (J2000)[a]	Dec (J2000)[a]	Telescope[b]	Line	Rest λ	Obs λ[c]	z	Note[d]
IVS B0812−252	08 14 55.1299	−25 21 43.924	NTT	Mg II	2799.9	5086.7	0.8167 ± 0.0002	
				Hγ	4340.5	[7903.2]		
IVS B0814−029	08 17 27.4860	−03 07 37.311	NTT	Si IV	1398.3	[3897.6]	1.7748 ± 0.0028	
				C IV	1549.5	4301.3		
				C III]	1908.7	5286.2		
				Mg II	2799.9	7781.0		
IVS B0838−573	08 40 09.0201	−57 32 02.320	NTT	C IV	1549.5	3764.9	1.4264 ± 0.0017	*
				He II	1640.4	[3999.0]		
				C III]	1908.7	4627.8		
				Mg II	2799.9	6789.3		
IVS B0845−837	08 40 09.6134	−83 54 32.576	NTT	Mg II	2799.9	4854.9	0.7344 ± 0.0005	
				Hδ	4101.7	7115.5		
				Hγ	4340.5	[7536.3]		
				Hβ	4861.3	8436.7		
				[O III]	4958.9	[8600.5]		
				[O III]	5006.8	8678.8		

Table 1—Continued

Source	RA (J2000)[a]	Dec (J2000)[a]	Telescope[b]	Line	Rest λ	Obs λ[c]	z	Note[d]
IVS B0855−716	08 55 11.7699	−71 49 06.457	NTT	Si IV	1398.3	[4000.6]	1.856 ± 0.003	
				C IV	1549.5	4431.3		
				C III]	1908.7	5438.2		
				Mg II	2799.9	8001.2		
IVS B0858−313	09 00 44.2942	−31 31 28.577	NTT	Mg II	2799.9	4064.7	0.4528 ± 0.0008	*
				Hβ	4861.3	7070.5		
				[O III]	5006.8	7271.2		
IVS B0905−202	09 07 54.0404	−20 26 49.475	NTT	Mg II	2799.9	5337.4	0.906 ± 0.003	S
IVS B0917−354	09 19 06.8892	−35 38 27.040	NTT	Mg II	2799.9	3861.0	0.3823 ± 0.0013	*
				Hδ	4101.7	5670.2		
				Hγ	4340.5	6000.4		
				Hβ	4861.3	6735.1		
				[O III]	5006.8	[6941.9]		
IVS B0922−202	09 25 11.9473	−20 27 35.610	NTT	C III]	1908.7	3975.0	1.0844 ± 0.0019	
				Mg II	2799.9	5841.3		
IVS B0937−187	09 39 21.2577	−18 58 05.738	NTT	Mg II	2799.9	4532.4	0.6207 ± 0.0014	

Table 1—Continued

Source	RA (J2000)[a]	Dec (J2000)[a]	Telescope[b]	Line	Rest λ	Obs λ[c]	z	Note[d]
				[Ne V]	3425.5	[5559.1]		
				Hγ	4340.5	7051.4		
				Hβ	4861.3	7893.5		
				[O III]	4958.9	8022.0		
				[O III]	5006.8	8104.4		
IVS B1006−093	10 08 43.8653	−09 33 23.359	NTT	C III]	1908.7	4247.5	1.2255 ± 0.0003	*
				Mg II	2799.9	6231.9		
IVS B1020−045	10 22 44.1124	−04 43 36.451	NTT	Lyβ	1025.7	[3730.5]	2.624 ± 0.005	
				Lyα	1215.7	4399.8		
				N V	1240.1	[4483.9]		
				Si IV	1398.3	5086.0		
				C IV	1549.5	5605.7		
				Si III]	1890.0	6845.5		
				C III]	1908.7	[6924.0]		
IVS B1044−512	10 46 38.9030	−51 30 11.063	NTT	Lyα	1215.7	4508.6	2.698 ± 0.006	
				Si IV	1398.3	[5194.1]		

Table 1—Continued

Source	RA (J2000)[a]	Dec (J2000)[a]	Telescope[b]	Line	Rest λ	Obs λ[c]	z	Note[d]
				C IV	1549.5	5723.6		
				C III]	1908.7	7043.7		
IVS B1046−463	10 48 18.0083	−46 39 17.458	NTT	N V	1240.1	[3738.9]	2.0129 ± 0.0010	
				Si IV	1398.3	4216.5		
				C IV	1549.5	4668.8		
				C III]	1908.7	5746.6		
				Mg II	2799.9	8433.7		
IVS B1115−111	11 17 34.0736	−11 23 50.717	NTT	C III]	1908.7	3753.9	0.9667 ± 0.0006	
				Mg II	2799.9	5512.7		
				[O II]	3726.8	7326.5		
				Hϵ	3970.1	7805.2		
				Hδ	4101.7	8063.8		
				Hγ	4340.5	[8571.0]		
IVS B1145−478	11 48 15.6570	−48 05 38.431	NTT	C III]	1908.7	4437.8	1.328 ± 0.003	
				Mg II	2799.9	6527.6		
IVS B1219−457	12 21 46.7644	−45 59 06.392	GS	[Ne IV]	2423.8	4971.1	1.052 ± 0.001	*

Table 1—Continued

Source	RA (J2000)[a]	Dec (J2000)[a]	Telescope[b]	Line	Rest λ	Obs λ[c]	z	Note[d]
				Mg II	2799.9	5744.9		
				[Ne V]	3425.5	7033.7		
IVS B1228−352	12 31 16.5421	−35 33 18.916	NTT	Mg II	2799.9	4993.7	0.7847 ± 0.0006	
				Hγ	4340.5	7753.8		
				Hβ	4861.3	8676.7		
				[O III]	4958.9	[8834.8]		
				[O III]	5006.8	8933.0		
IVS B1229−123	12 31 50.2657	−12 36 37.056	NTT	Lyα	1215.7	3819.6	2.115 ± 0.009	
				C IV	1549.5	4816.8		
				C III]	1908.7	5926.5		
				Mg II	2799.9	8696.5		
IVS B1236−381	12 38 52.7315	−38 25 56.991	NTT	C IV	1549.5	3870.1	1.4974 ± 0.0010	
				He II	1640.4	[4099.7]		
				C III]	1908.7	4763.4		
				Mg II	2799.9	6996.6		
IVS B1320−385	13 23 04.1483	−38 49 00.671	GS	C IV	1549.5	4977.5	2.2127 ± 0.0005	

Table 1—Continued

Source	RA (J2000)[a]	Dec (J2000)[a]	Telescope[b]	Line	Rest λ	Obs λ[c]	z	Note[d]
				C III]	1908.7	6132.9		
IVS B1418−481	14 21 38.6465	−48 20 22.796	GS	C IV	1549.5	4409.9	1.851 ± 0.005	*
				C III]	1908.7	5450.2		
IVS B1520−334	15 23 54.0398	−33 38 45.236	GS	Mg II	2799.9	4575.5	0.6343 ± 0.0002	
				[Ne V]	3425.5	5600.2		
				[Ne III]	3868.7	6323.2		
				Hζ	3889.0	6357.6		
				Hϵ	3970.1	6485.8		
				Hδ	4101.7	6705.9		
				Hγ	4340.5	7094.1		
				[O III]	4363.2	7127.5		
IVS B1531−225	15 34 22.8012	−22 43 57.629	GS	Mg II	2799.9	5546.9	0.981 ± 0.002	S
IVS B1540−828	15 50 59.1404	−82 58 06.838	GS	C IV	1549.5	4243.7	1.7383 ± 0.0006	
				C III]	1908.7	5226.1		
				C II]	2326.9	6368.2		
				[Ne IV]	2423.8	6640.0		

Table 1—Continued

Source	RA (J2000)[a]	Dec (J2000)[a]	Telescope[b]	Line	Rest λ	Obs λ[c]	z	Note[d]
IVS B1541−230	15 44 14.1780	−23 12 01.347	GS	Lyα	1215.7	4462.0	2.664 ± 0.004	
				C IV	1549.5	5668.6		
				C III]	1908.7	6989.8		
IVS B1545−760	15 52 20.4427	−76 14 46.933	GS	[O II]	3726.8	4575.9	0.2273 ± 0.0002	
				[Ne III]	3868.7	[4752.5]		
				Hγ	4340.5	[5338.1]		
				Hβ	4861.3	5965.5		
				[O III]	4958.9	6085.6		
				[O III]	5006.8	6144.4		
IVS B1558−072	16 00 56.4765	−07 22 05.224	GS	Si IV	1398.3	4197.6	2.0016 ± 0.0002	*
				C IV	1549.5	4650.3		
				He II	1640.4	[4921.0]		
				C III]	1908.7	5729.7		
IVS B1606−742	16 12 33.8838	−74 23 40.137	GS	Mg II	2799.9	4603.3	0.6453 ± 0.0005	
				[Ne V]	3425.5	5640.8		
				[O II]	3726.8	6131.4		

Table 1—Continued

Source	RA (J2000)[a]	Dec (J2000)[a]	Telescope[b]	Line	Rest λ	Obs λ[c]	z	Note[d]
				[Ne III]	3868.7	6365.3		
				Hγ	4340.5	[7155.8]		
IVS B1621+058	16 24 07.7338	+05 43 24.244	GS	C III]	1908.7	4821.7	1.5273 ± 0.0012	
				Mg II	2799.9	7079.5		
IVS B1628−771	16 36 02.9612	−77 13 34.420	GS	[O II]	3726.8	5072.3	0.3605 ± 0.0001	
				[Ne III]	3868.7	5263.6		
				Hβ	4861.3	6612.8		
				[O III]	4958.9	6746.2		
				[O III]	5006.8	6811.3		
IVS B1643+007	16 46 06.9722	+00 42 27.279	GS	C III]	1908.7	4530.0	1.3726 ± 0.0008	
				Mg II	2799.9	6640.9		
IVS B1700−577	17 04 18.0630	−57 51 01.604	GS	[Ne V]	3425.5	[4738.9]	0.3833 ± 0.0001	
				[O II]	3726.8	5154.0		
				[Ne III]	3868.7	5352.7		
				[Ne III]	3967.4	[5488.7]		
				Hδ	4101.7	[5666.0]		

Table 1—Continued

Source	RA (J2000)[a]	Dec (J2000)[a]	Telescope[b]	Line	Rest λ	Obs λ[c]	z	Note[d]
				Hγ	4340.5	[6017.0]		
				[O III]	4363.2	6034.0		
				Hβ	4861.3	6726.3		
				[O III]	4958.9	6859.7		
				[O III]	5006.8	6927.0		
IVS B1701−132	17 04 05.0868	−13 16 34.234	GS	Lyα	1215.7	[4254.8]	2.4916 ± 0.0010	
				C IV	1549.5	5408.7		
				C III]	1908.7	6666.3		
IVS B1712+530	17 13 49.8706	+53 00 32.790	GN	Si IV	1398.3	4529.4	2.233 ± 0.003	*
				C IV	1549.5	4996.9		
				Si III]	1890.0	6116.1		
				C III]	1908.7	6166.3		
IVS B1717−618	17 21 39.0167	−61 54 43.020	GS	Mg II	2799.9	4643.4	0.6579 ± 0.0002	
				[Ne V]	3425.5	5679.4		
				[O II]	3726.8	6177.1		
				[Ne III]	3868.7	6412.8		

Table 1—Continued

Source	RA (J2000)[a]	Dec (J2000)[a]	Telescope[b]	Line	Rest λ	Obs λ[c]	z	Note[d]
				Hγ	4340.5	[7216.1]		
IVS B1800−709	18 06 23.6852	−70 58 28.762	GS	C III]	1908.7	[4398.4]	1.303 ± 0.001	S
				Mg II	2799.9	6449.3		
IVS B1810−745	18 16 40.0762	−74 29 07.343	GS	C IV	1549.5	5035.6	2.256 ± 0.006	*
				C III]	1908.7	6224.7		
IVS B1813−497	18 16 55.9942	−49 43 44.671	GS	C IV	1549.5	4176.9	1.697 ± 0.002	*
				C III]	1908.7	5151.2		
IVS B1905−252	19 08 48.4392	−25 09 29.373	GS	C IV	1549.5	4095.7	1.6434 ± 0.0003	*
				C III]	1908.7	5045.9		
IVS B1905−794	19 13 33.2602	−79 20 14.810	GS	Mg II	2799.9	5720.7	1.043 ± 0.001	S
IVS B1939−316	19 42 40.9140	−31 30 14.609	GS	C III]	1908.7	4927.5	1.5818 ± 0.0002	
				Mg II	2799.9	7229.2		
IVS B1941−372	19 44 57.8355	−37 07 09.874	GS	C IV	1549.5	4396.2	1.840 ± 0.002	
				He II	1640.4	[4669.8]		
				C III]	1908.7	5424.5		
IVS B1957−423	20 00 56.7918	−42 14 46.269	GS	Mg II	2799.9	5575.9	0.9889 ± 0.0025	*

Table 1—Continued

Source	RA (J2000)[a]	Dec (J2000)[a]	Telescope[b]	Line	Rest λ	Obs λ[c]	z	Note[d]
				[Ne V]	3425.5	6804.5		
IVS B2029−215	20 32 54.3154	−21 25 15.756	GS	Mg II	2799.9	5241.0	0.8722 ± 0.0004	*
				[O II]	3726.8	6978.9		
IVS B2036−034	20 39 09.9852	−03 17 14.411	GS	C III]	1908.7	[4872.3]	1.551 ± 0.002	S *
				Mg II	2799.9	7142.6		
IVS B2039−078	20 42 04.9182	−07 42 37.845	GS	Mg II	2799.9	5727.0	1.045 ± 0.001	S
IVS B2044−188	20 47 37.6552	−18 41 41.352	GS	Lyβ	1025.7	[4128.5]	3.002 ± 0.004	*
				Lyα	1215.7	4873.8		
				N V	1240.1	4949.1		
				Si II	1265.2	[5070.2]		
				O I/Si II	1305.4	5235.7		
				Si IV	1398.3	5595.6		
				C IV	1549.5	6187.7		
IVS B2048−557	20 52 13.6851	−55 33 10.043	GS	C III]	1908.7	[4771.4]	1.502 ± 0.002	S
				Mg II	2799.9	7005.6		
IVS B2051−204	20 54 22.0724	−20 16 16.819	GS	Mg II	2799.9	5577.8	0.992 ± 0.001	S

Table 1—Continued

Source	RA (J2000)[a]	Dec (J2000)[a]	Telescope[b]	Line	Rest λ	Obs λ[c]	z	Note[d]
IVS B2107−553	21 11 12.1527	−55 08 06.172	GS	Lyα	1215.7	[4141.2]	2.3965 ± 0.0005	*
				Si IV	1398.3	[4756.3]		
				C IV	1549.5	5262.2		
				C III]	1908.7	6483.8		
IVS B2118−037	21 20 48.4735	−03 30 28.929	GS	C IV	1549.5	4207.2	1.7169 ± 0.0017	
				C III]	1908.7	5188.9		
IVS B2131−340	21 34 50.8245	−33 51 14.750	GS	C IV	1549.5	4206.0	1.7150 ± 0.0006	
				C III]	1908.7	5183.2		
IVS B2131−690	21 35 49.8826	−68 48 33.925	GS	C III]	1908.7	4688.6	1.464 ± 0.008	*
				Mg II	2799.9	6922.2		
IVS B2132−638	21 36 22.0749	−63 35 51.038	GS	C III]	1908.7	4835.6	1.537 ± 0.004	*
				Mg II	2799.9	7113.7		
IVS B2137−644	21 41 46.4411	−64 11 14.476	GS	[Ne V]	3425.5	[6704.1]	0.959 ± 0.003	S
				Mg II	2799.9	5484.8		
IVS B2155−475	21 58 40.2025	−47 19 26.552	GS	C IV	1549.5	4238.6	1.7371 ± 0.0017	*
				C III]	1908.7	5227.5		

Table 1—Continued

Source	RA (J2000)[a]	Dec (J2000)[a]	Telescope[b]	Line	Rest λ	Obs λ[c]	z	Note[d]
IVS B2157−255	21 59 50.7922	−25 16 52.176	GS	Mg II	2799.9	4693.7	0.6757 ± 0.0002	
				[Ne V]	3425.5	5738.7		
				[O II]	3726.8	6245.1		
				[Ne III]	3868.7	6481.8		
IVS B2211+069	22 14 08.8615	+07 11 42.393	GN	[O II]	3726.8	5373.0	0.4412 ± 0.0004	
				[O III]	4958.9	7143.3		
				[O III]	5006.8	7212.7		
				Mg b	5175.0	7462.9		
IVS B2225−694	22 29 00.1767	−69 10 30.274	GS	Mg II	2799.9	5340.0	0.907 ± 0.001	S
IVS B2226−634	22 30 10.3381	−63 10 43.299	GS	Lyα	1215.7	4111.8	2.3841 ± 0.0010	
				N V	1240.1	[4191.8]		
				Si IV	1398.3	[4730.4]		
				C IV	1549.5	5245.9		
				C III]	1908.7	6459.9		
IVS B2235−556	22 39 06.0344	−55 25 59.410	GS	C IV	1549.5	4599.6	1.9706 ± 0.0022	
				He II	1640.4	[4874.0]		

Table 1—Continued

Source	RA (J2000)[a]	Dec (J2000)[a]	Telescope[b]	Line	Rest λ	Obs λ[c]	z	Note[d]
				C III]	1908.7	5674.1		
IVS B2243−081	22 45 49.0038	−07 55 19.381	GS	C IV	1549.5	4347.3	1.8069 ± 0.0005	
				Al III	1857.4	5214.0		
				Si III]	1890.0	5307.0		
				C III]	1908.7	5357.4		
IVS B2250+323	22 53 12.4997	+32 36 04.326	GN	[O II]	3726.8	4686.3	0.2580 ± 0.0004	
				[Ne III]	3868.7	4865.9		
				[Ne III]	3967.4	4990.5		
				Hϵ	3971.2	5008.2		
				Hδ	4101.7	5156.4		
				Hγ	4340.5	5462.4		
				[O III]	4363.2	5489.0		
				Hβ	4861.3	6114.6		
				[O III]	4958.9	6233.5		
				[O III]	5006.8	6294.9		
IVS B2255−705	22 58 31.5632	−70 14 39.728	NTT	C III]	1908.7	3956.9	1.077 ± 0.004	

Table 1—Continued

Source	RA (J2000)[a]	Dec (J2000)[a]	Telescope[b]	Line	Rest λ	Obs λ[c]	z	Note[d]
				Mg II	2799.9	5826.9		
IVS B2300+386	23 03 04.0658	+38 53 48.365	GN	C IV	1549.5	4253.4	1.7462 ± 0.0013	*
				C III]	1908.7	5244.2		
IVS B2311+276	23 13 54.8539	+27 57 04.514	GN	Lyα	1215.7	[4651.2]	2.801 ± 0.006	
				Si IV	1398.3	[5293.9]		
				C IV	1549.5	5880.7		
				C III]	1908.7	7267.4		
IVS B2313−182	23 15 48.1321	−18 00 40.251	NTT	[O II]	3726.8	5270.3	0.4126 ± 0.0013	*
				[O III]	4958.9	7013.4		
				[O III]	5006.8	7080.2		
				Ca K	3934.8	5559.9		
				Ca H	3969.6	5586.6		
IVS B2317−372	23 19 53.5643	−36 56 28.265	NTT	Mg II	2799.9	4140.0	0.4805 ± 0.0005	
				[O II]	3726.8	5519.4		
				Hβ	4861.3	7197.7		
				[O III]	4958.9	7344.5		

Table 1—Continued

Source	RA (J2000)[a]	Dec (J2000)[a]	Telescope[b]	Line	Rest λ	Obs λ[c]	z	Note[d]
				[O III]	5006.8	7416.1		

[a]ICRF2 radio position

[b]Telescope abbreviations: GN = Gemini North, GS = Gemini South, NTT = ESO New Technology Telescope

[c]Square brackets indicate the line was not used for redshift determination

[d]"S" denotes a single-line redshift; * indicates a note in Section 3.1

Table 2. Probable BL Lac objects

Source	RA (J2000)[a]	Dec (J2000)[a]	Telescope
IVS B0019−261	00 21 32.5495	−25 50 49.387	GS
IVS B0138−381	01 40 36.8208	−37 56 45.798	NTT
IVS B0141+268	01 44 33.5538	+27 05 03.119	GN
IVS B0142−590	01 43 47.4305	−58 45 51.375	NTT
IVS B0258−170	03 01 16.6227	−16 52 45.101	GS
IVS B0839−357	08 41 21.6331	−35 55 05.967	NTT
IVS B0843−547	08 45 02.4822	−54 58 08.545	NTT
IVS B1029−854	10 26 34.3753	−85 43 14.295	NTT
IVS B1101−536	11 03 52.2217	−53 57 00.697	NTT
IVS B1304−427	13 07 37.9835	−42 59 38.987	NTT
IVS B1711−670	17 16 22.3365	−67 06 24.119	GS
IVS B2257+313	23 00 22.8374	+31 37 04.405	GN
IVS B2308+018	23 11 01.2929	+02 05 05.327	GN
IVS B2310+062	23 13 07.7015	+06 28 38.847	GN

[a]ICRF2 radio position

Table 3. Objects with low signal-to-noise spectra

Source	RA (J2000)[a]	Dec (J2000)[a]	Telescope
IVS B0002−350	00 05 05.9251	−34 45 49.656	NTT
IVS B0054−451	00 56 45.8532	−44 51 02.141	NTT, GS
IVS B0059−628	01 01 14.9683	−62 33 06.339	GS
IVS B0131−795	01 31 48.8223	−79 16 17.486	NTT
IVS B0253−754	02 53 10.8817	−75 13 16.686	GS
IVS B0255+203	02 58 07.3094	+20 30 01.580	GN
IVS B0302−063	03 05 00.5637	−06 07 41.500	GS
IVS B0312−512	03 14 25.7036	−51 04 31.562	GS
IVS B0545+221	05 48 03.8896	+22 10 35.593	GN
IVS B1004−500	10 06 14.0093	−50 18 13.471	GS
IVS B1151−324	11 54 06.1664	−32 42 42.983	NTT
IVS B1517−385	15 20 40.4844	−38 45 32.412	GS
IVS B1532−473	15 35 52.2412	−47 30 22.978	GS
IVS B1650−157	16 53 34.2064	−15 51 29.888	GS
IVS B1653−612	16 57 49.0093	−61 21 37.859	GS
IVS B1732−598	17 36 30.8521	−59 51 58.749	GS
IVS B1830−589	18 34 27.4734	−58 56 36.272	GS
IVS B1914−412	19 18 16.0574	−41 11 31.055	GS
IVS B1935−452	19 39 30.0868	−45 10 01.273	GS
IVS B2009+795	20 07 13.1610	+79 42 11.336	GN
IVS B2025−538	20 29 35.0553	−53 39 07.295	GS

Table 3—Continued

Source	RA (J2000)[a]	Dec (J2000)[a]	Telescope
IVS B2210+277	22 12 39.1030	+27 59 38.449	GN

[a]ICRF2 radio position

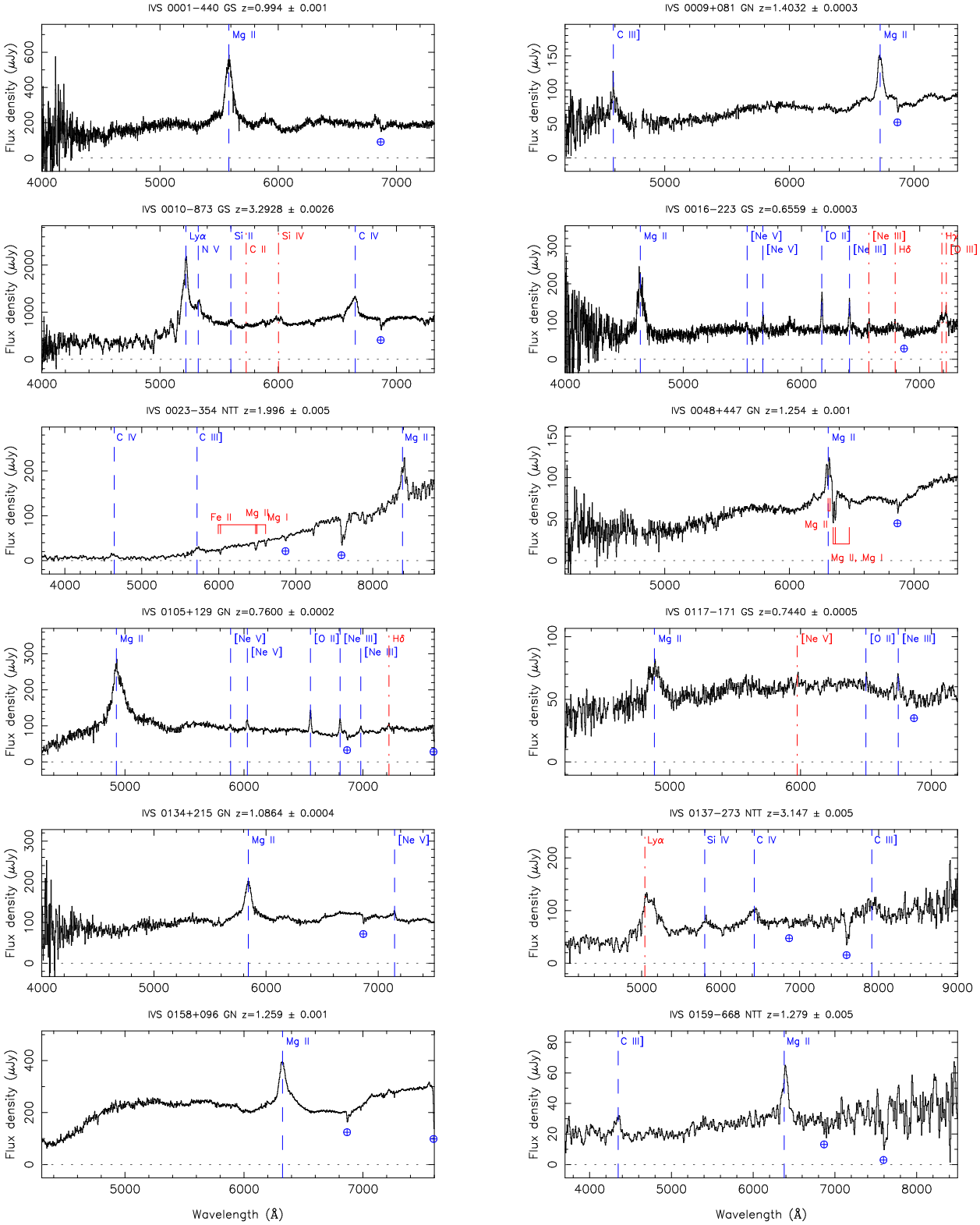

Fig. 1.— Optical spectra for 112 emission-line IVS targets. Dashed lines (blue) indicate emission lines used for redshift determination; dot-dashed lines (red) indicate lines detected at lower signal-to-noise or blended. Short gaps in Gemini spectra are due to physical gaps between the GMOS CCDs. Occasional longer gaps arise from calibration problems or strong

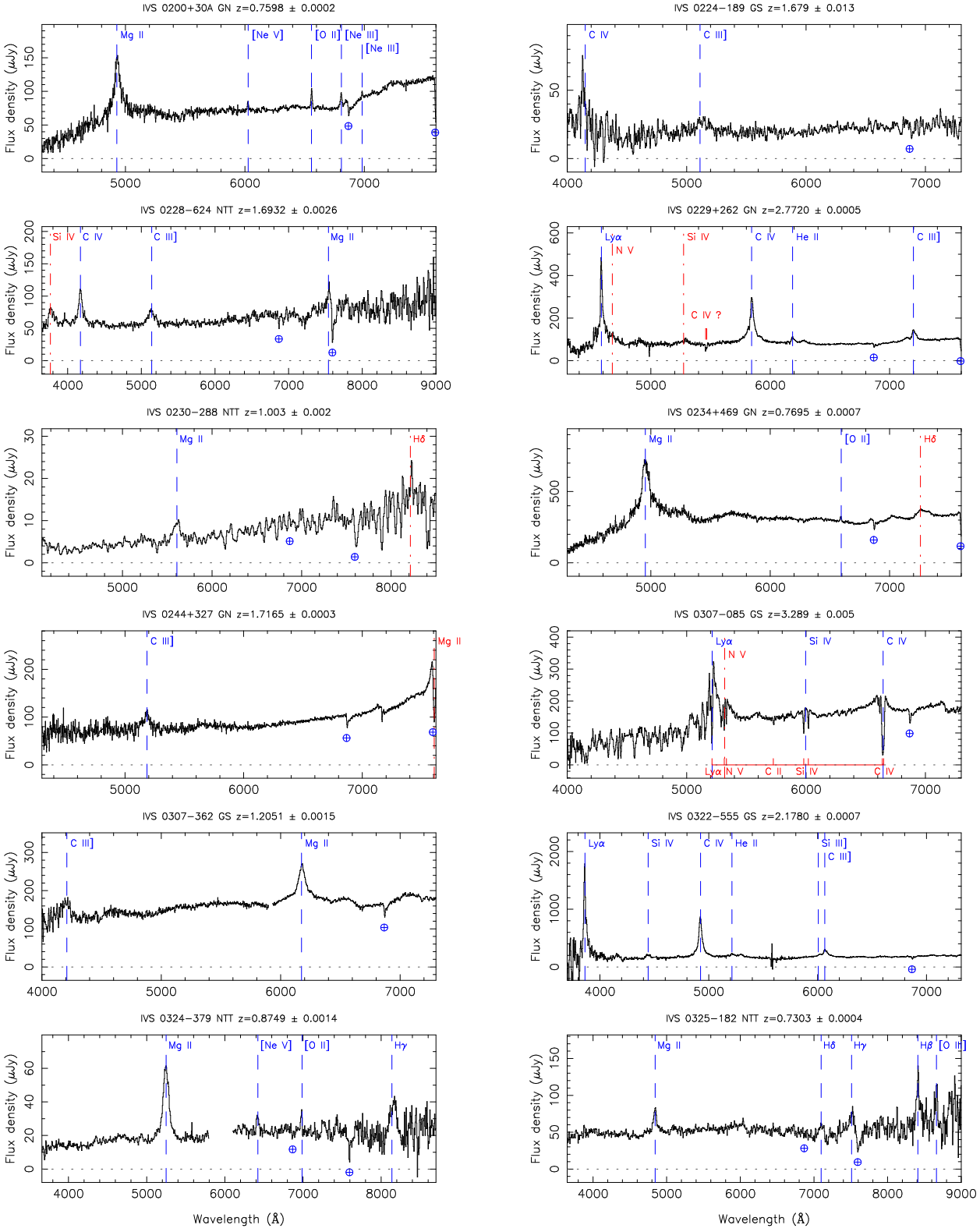

Fig. 1 (continued).—

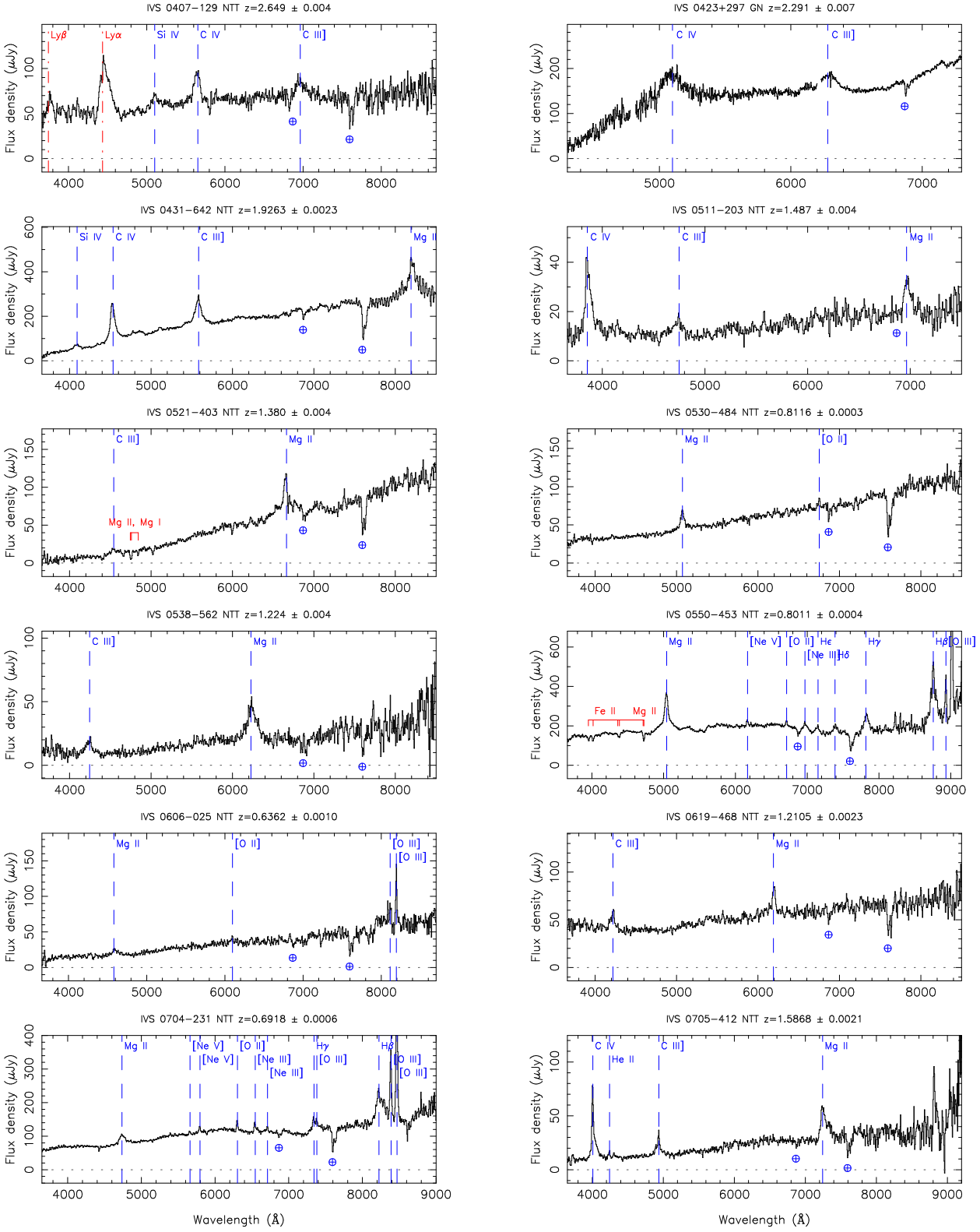

Fig. 1 (continued).—

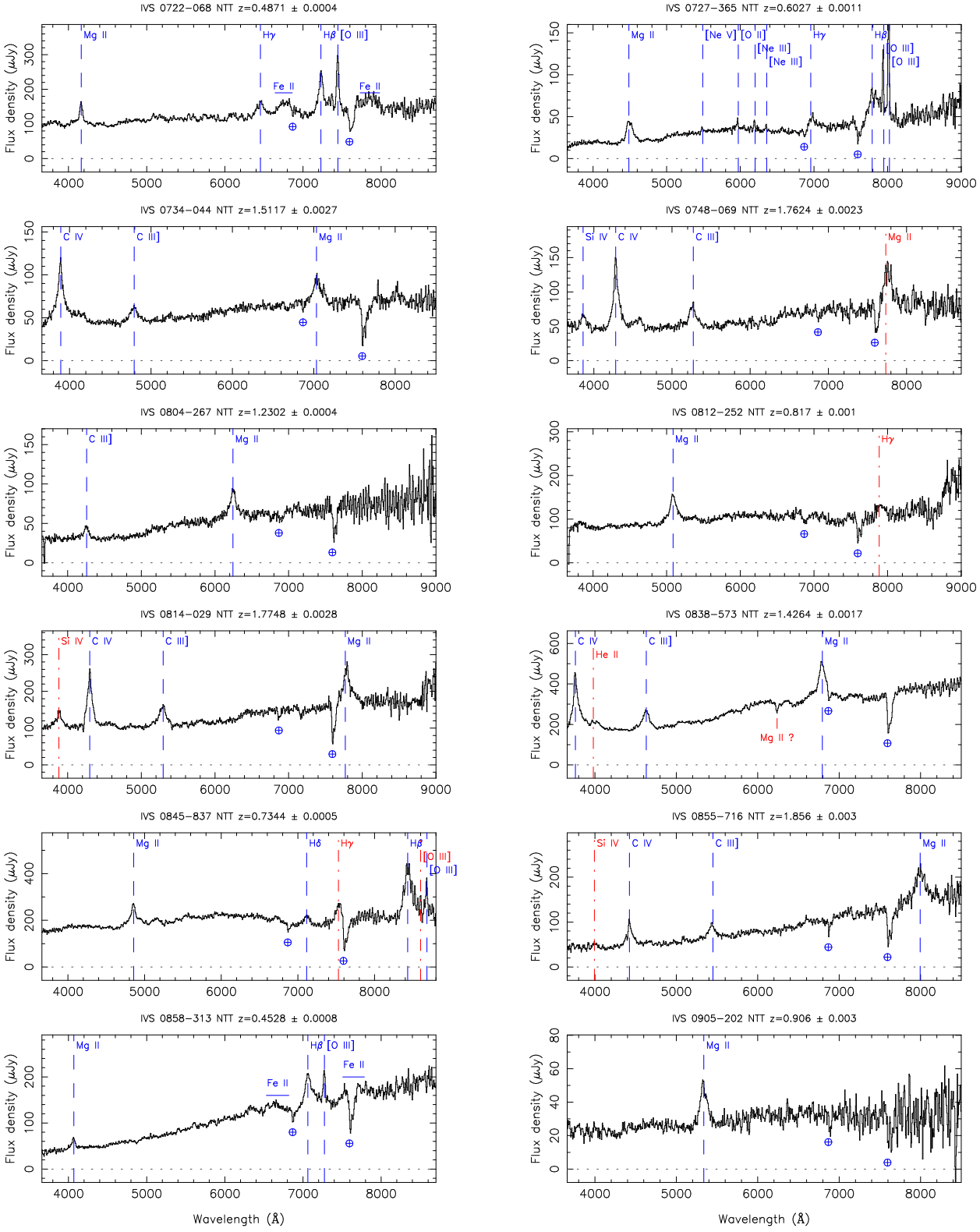

Fig. 1 (continued).—

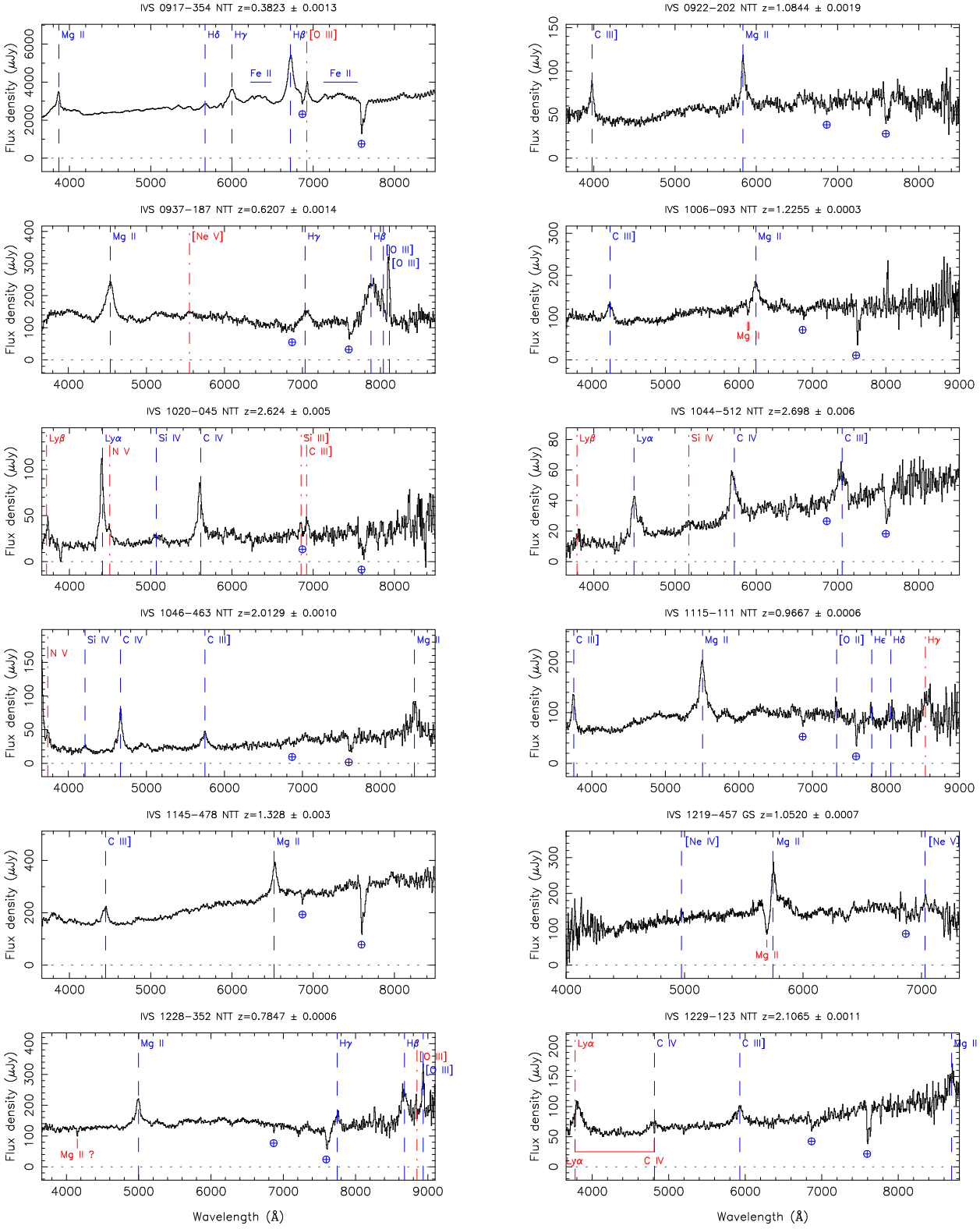

Fig. 1 (continued).—

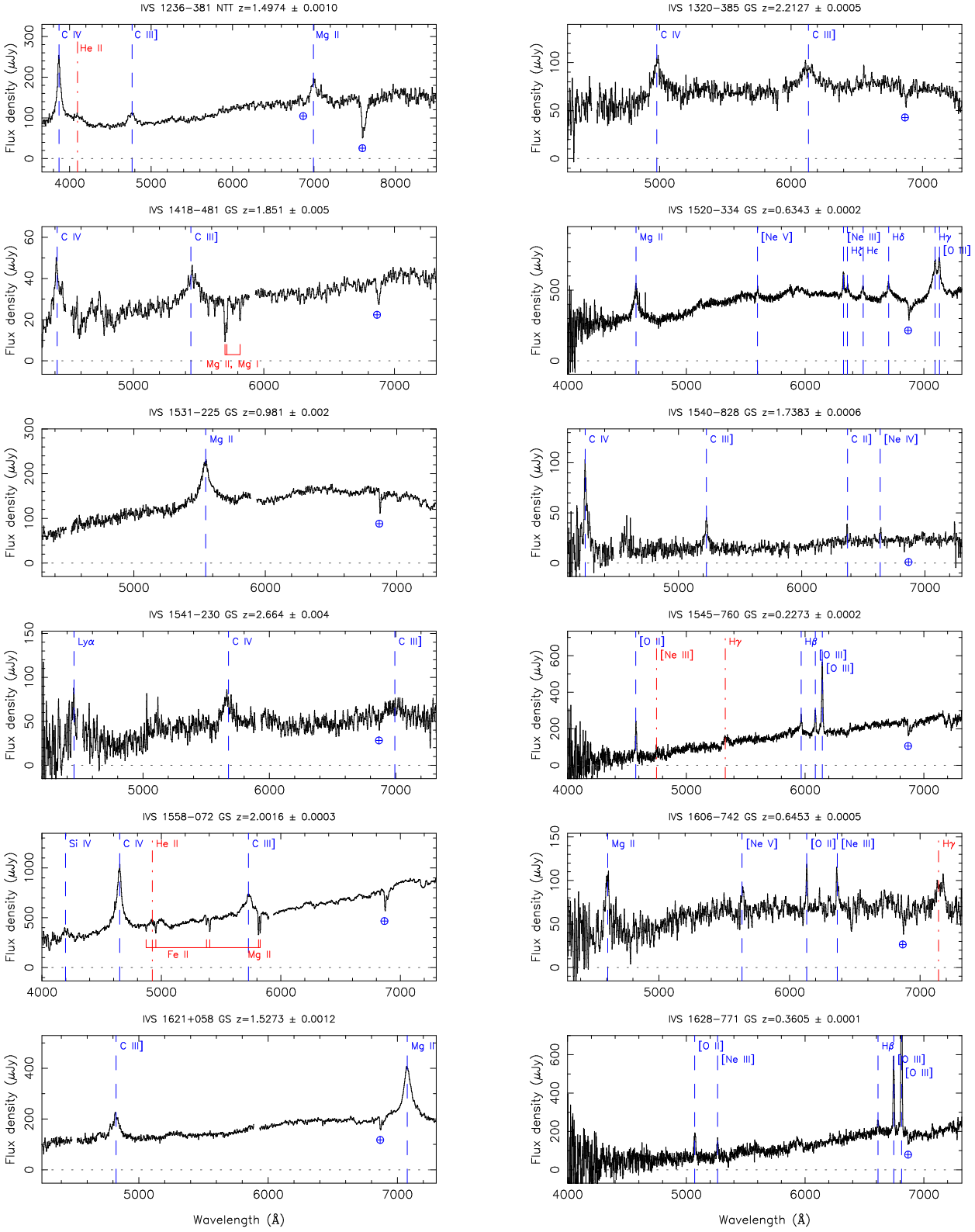

Fig. 1 (continued).—

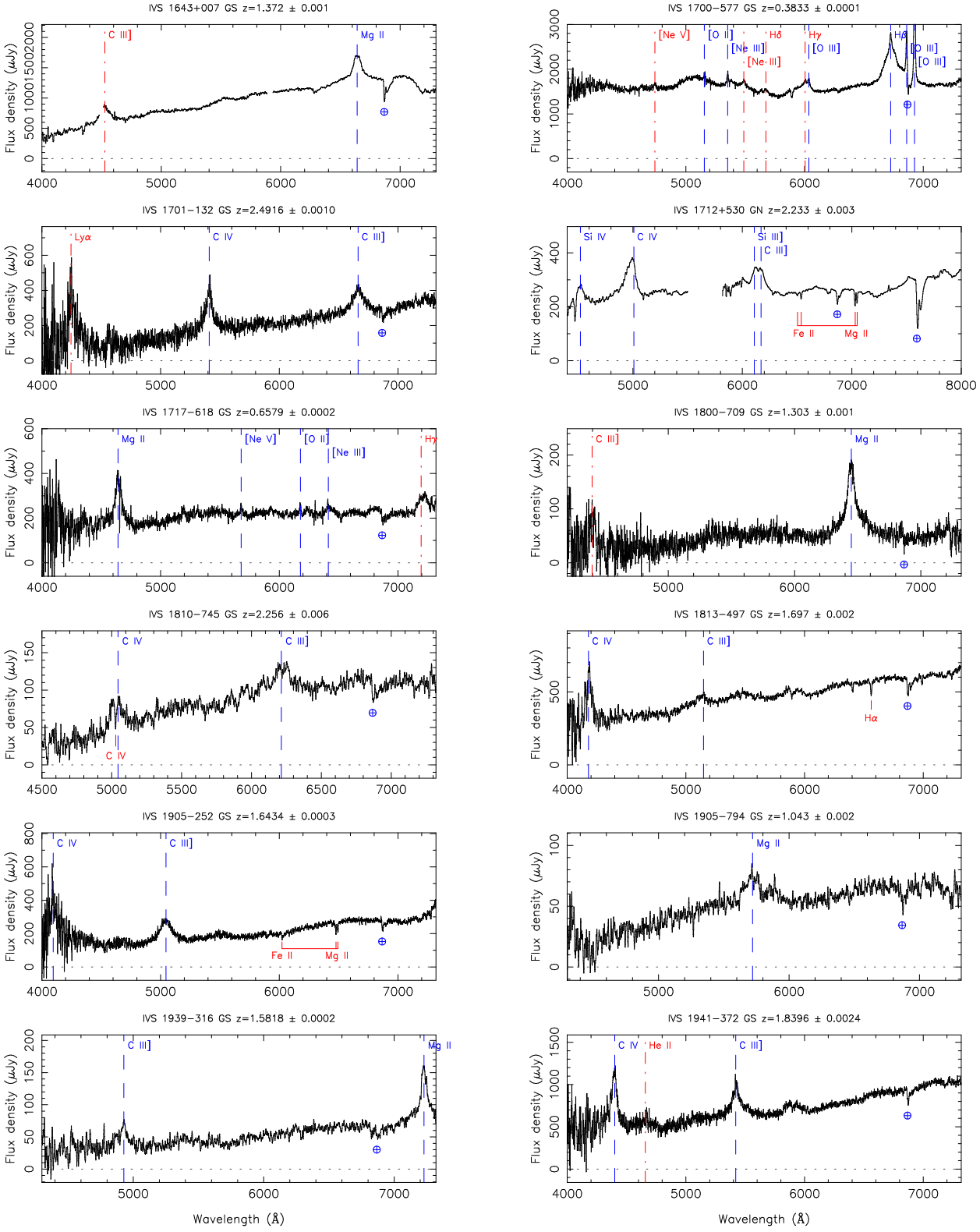

Fig. 1 (continued).—

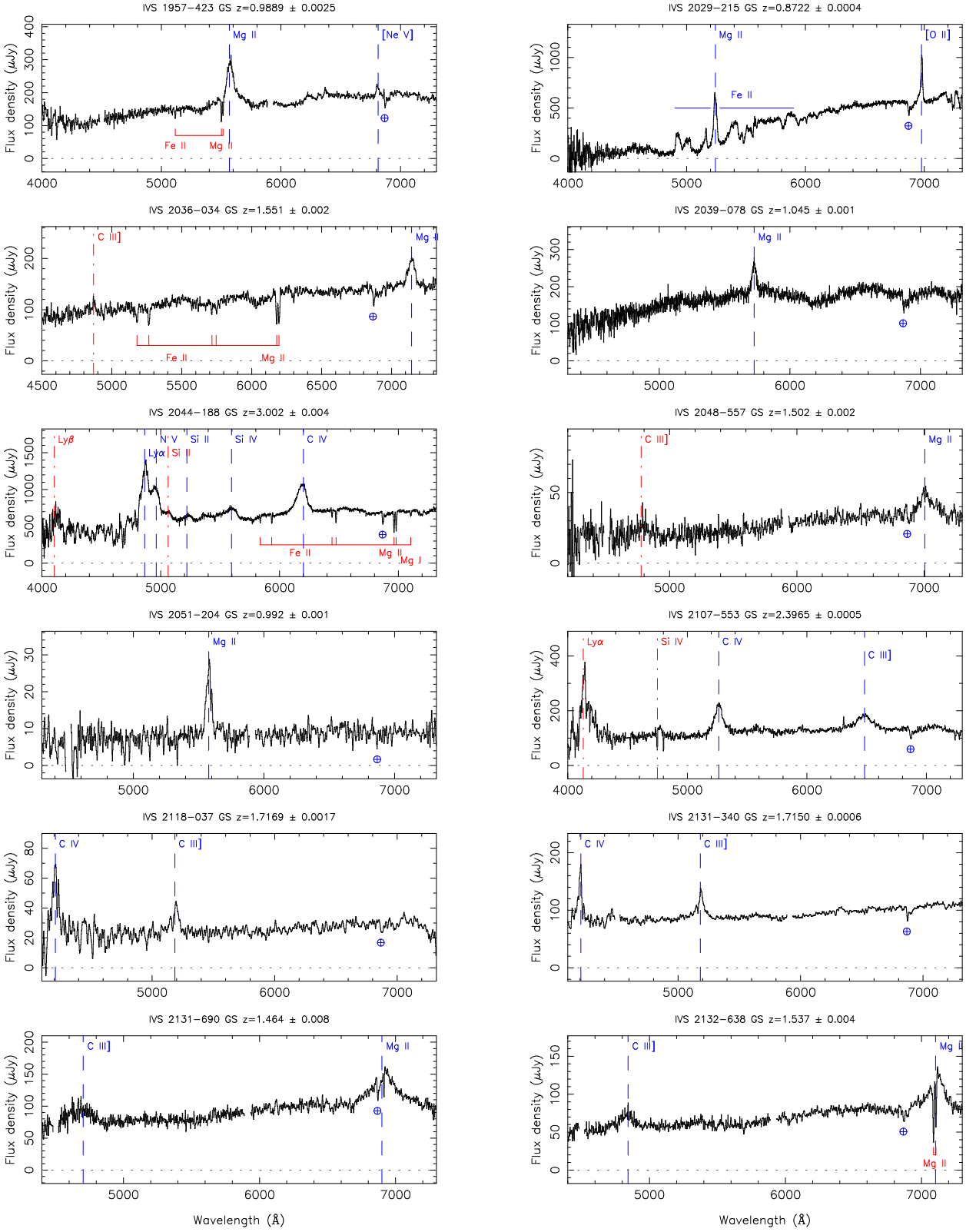

Fig. 1 (continued).—

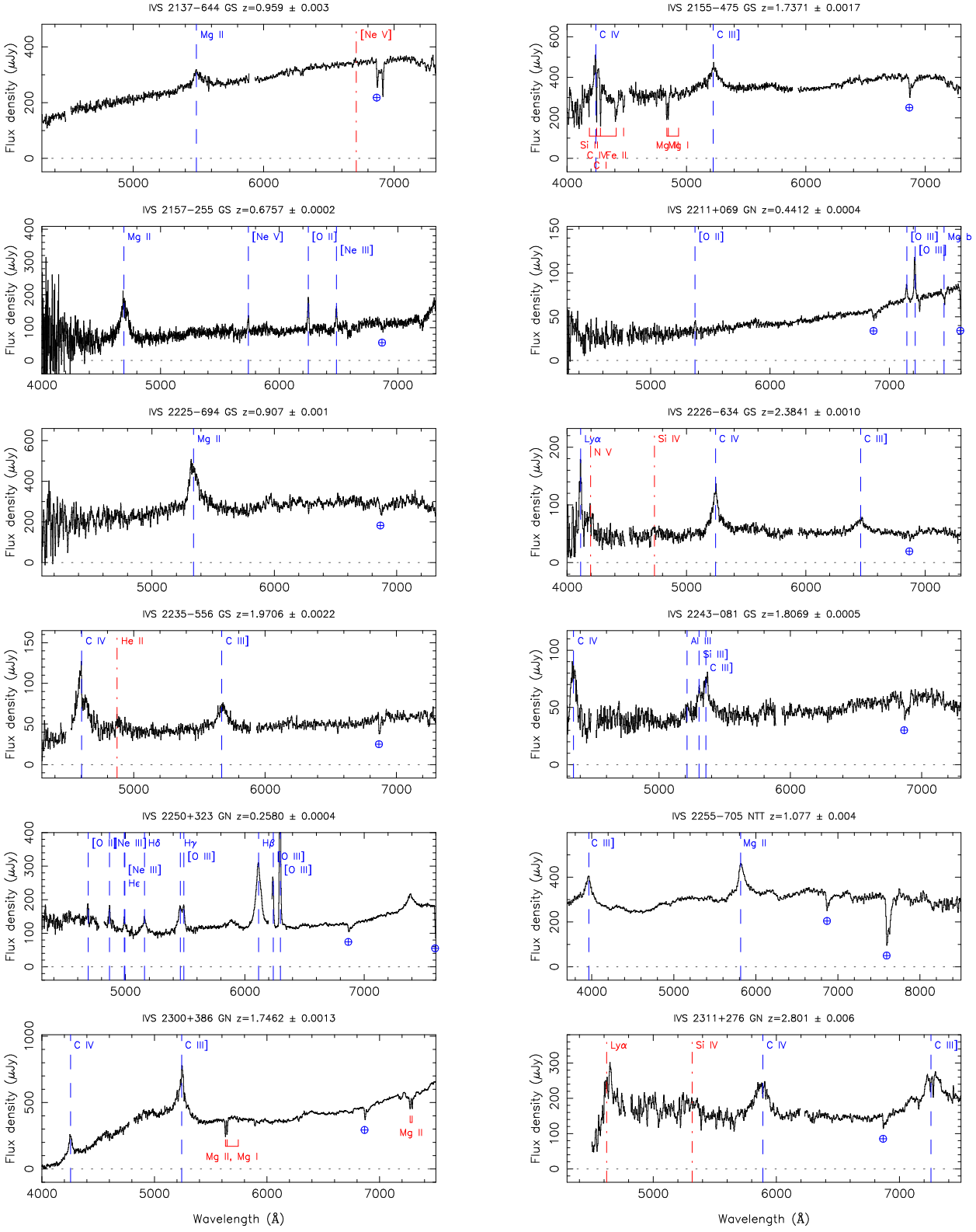

Fig. 1 (continued).—

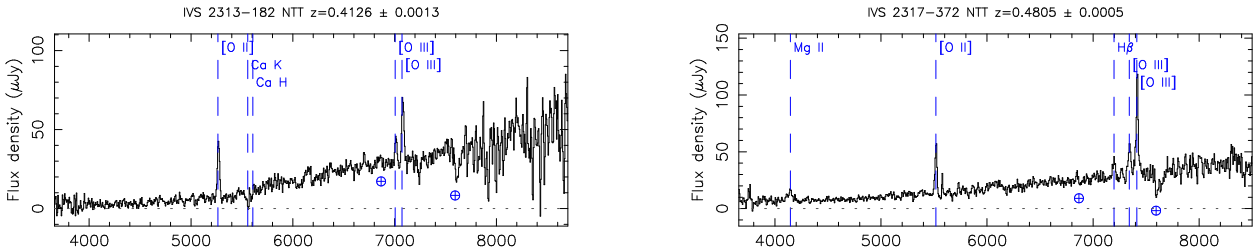

Fig. 1 (continued).—

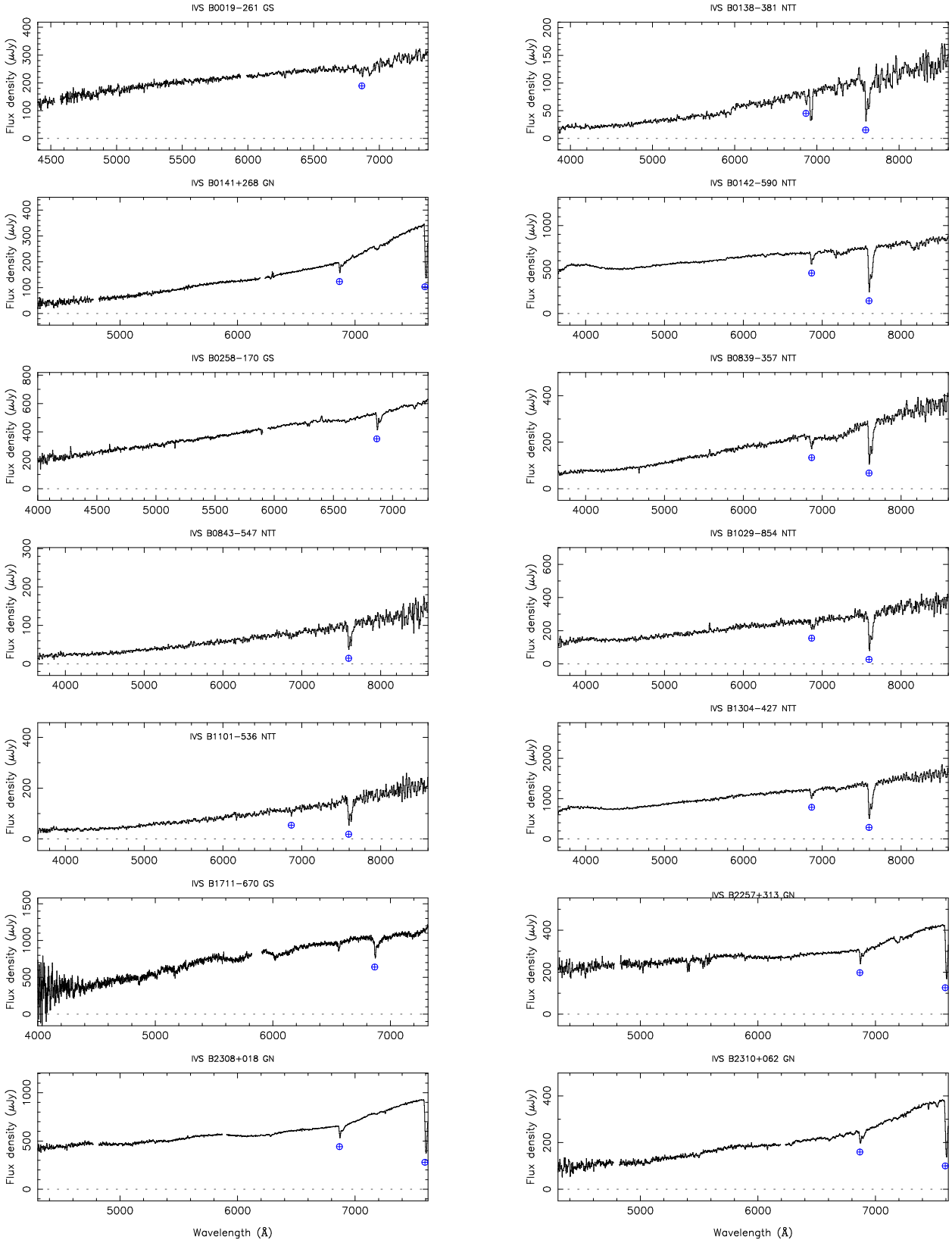

Fig. 2.— Spectra of 14 probable BL Lac objects from our observations, classified on the basis of their featureless spectra; see Table 2 for ICRF2 positions.

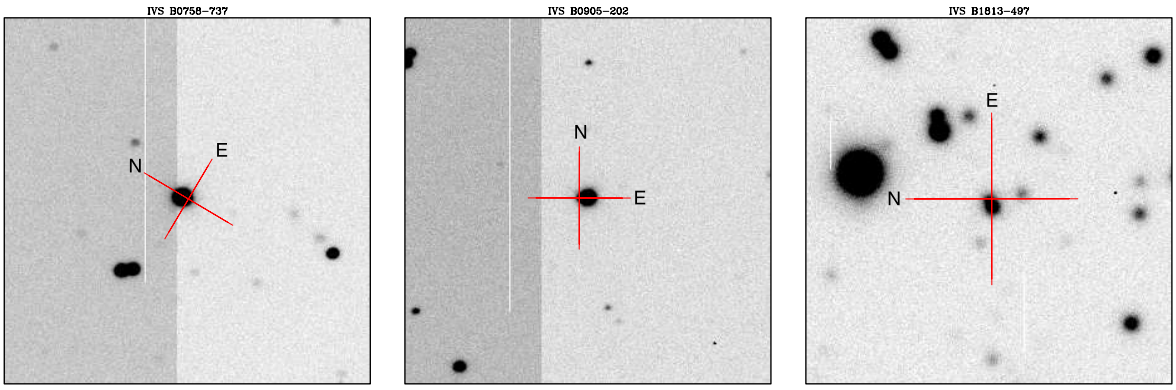

Fig. 3.— Acquisition images for the fields of IVS B0758−737, B0905−202, and B1813−497, all of which are partly obscured by a foreground star; position offsets between the radio source and obscuring star are 1.3″, 1.6″ and 0.8″, respectively. The arms of the cross marking the radio position are all 20 arcsec, and the orientation of each finding chart is indicated. The step in contrast in the two leftmost NTT images is the result of fast readout using two amplifiers.

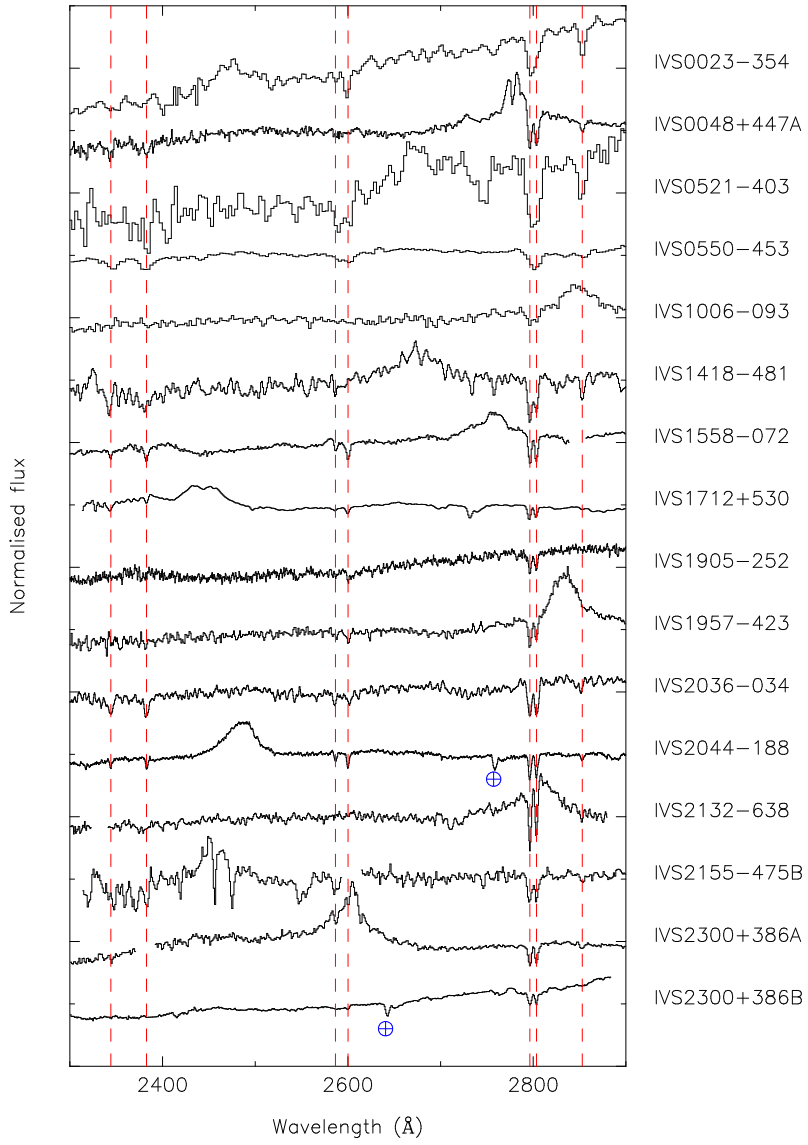

Fig. 4.— Montage of the Mg II absorption systems shifted back to the absorption rest frame. Telluric lines are marked and short spectral gaps correspond to gaps between the GMOS CCDs.

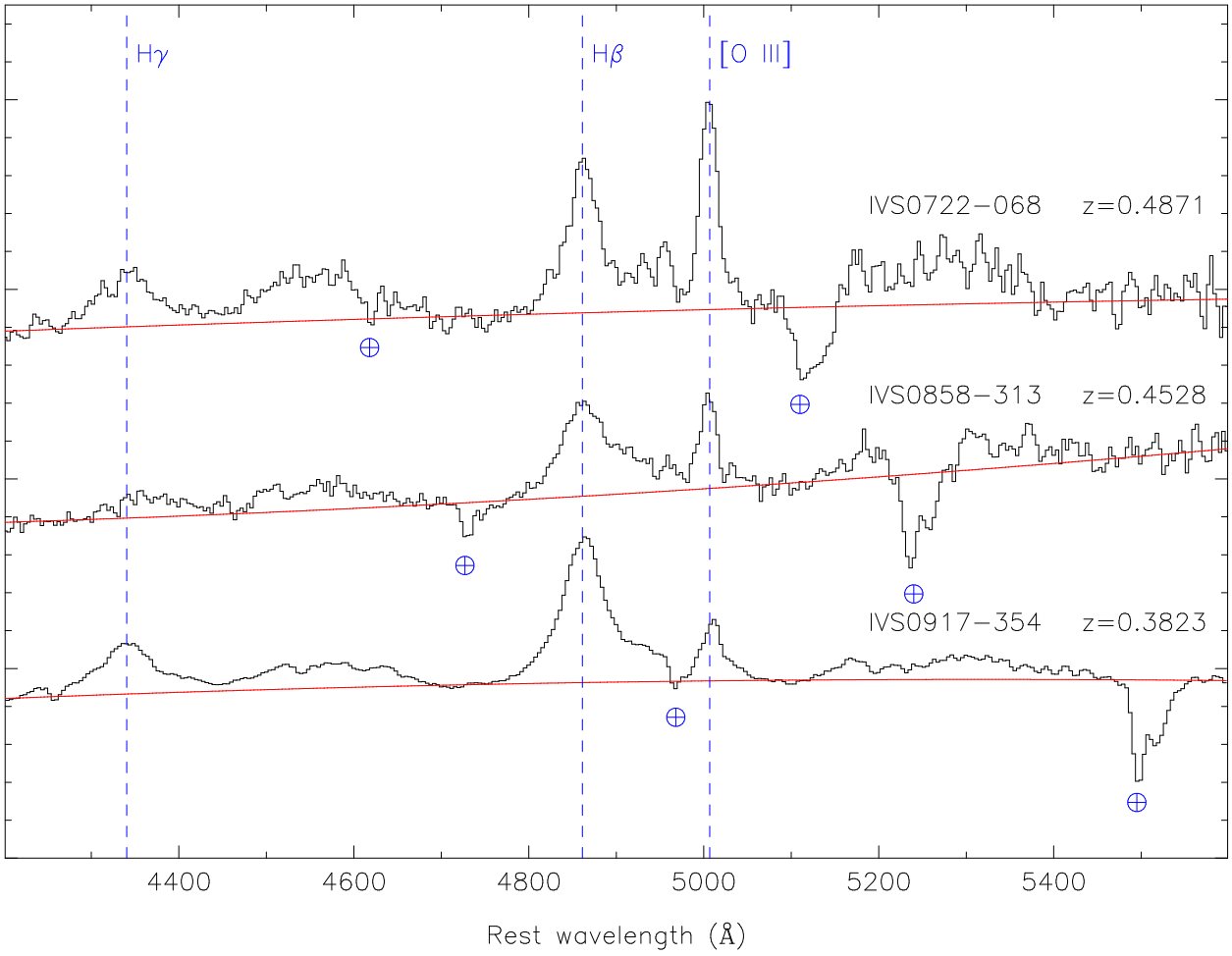

Fig. 5.— Montage of three $z \sim 0.4$ quasar spectra showing prominent broad Fe II emission both blueward and redward of Hβ. Spectra have been shifted to the rest frame and telluric features are marked. The effect of Fe II emission on the Hβ/[O III] profiles is most clearly seen in the high signal-to-noise spectrum of IVS B0917−354. The solid line (red) shows our estimated continuum level.

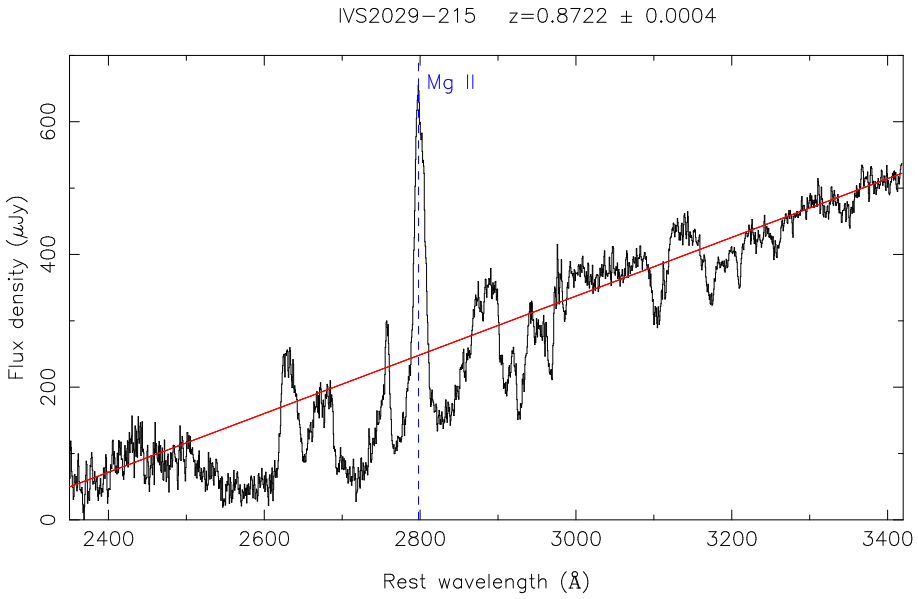

Fig. 6.— Optical spectrum of the $z = 0.8722$ FeLoBAL quasar IVS B2029−215 shifted to the emission rest frame. A tentative underlying continuum is shown (see text).